J Therm Spray Tech (2019) 28:1532–1553
https://doi.org/10.1007/s11666-019-00909-6

PEER REVIEWED

Characterization of the Gradient (Mo, Re)Si_2/Mo-Re Coatings Deposited in the Hybrid Process

Grzegorz Moskal[1] · **Damian Migas**[1] · **Małgorzata Osadnik**[2] · **Adriana Wrona**[2]

Submitted: 29 January 2019 / in revised form: 28 August 2019 / Published online: 6 September 2019

Abstract Novel siliconized Mo-Re coatings dedicated to applications in the glass industry are shown in this paper. The study aims at the characterization of morphology, phase composition, and oxidation behavior of siliconized Mo-based coatings deposited on a ceramic–metal substrate. Two coatings with different contents of rhenium were prepared using a hybrid process that includes atmospheric plasma spraying and pack siliconizing. The microstructure, chemical, and phase composition of the obtained coatings were characterized and compared to Mo coating. Moreover, a characterization of starting powders was performed. After the description of the coatings' microstructure, oxidation tests were carried out at 1000, 1100, and 1200 °C. The surface condition of oxidized coatings was investigated. The structure of Re-containing coatings after the siliconizing process was comparable. Both were composed of Mo and (Mo,Re)Si_2-$ReSi_{1.75}$ layers. However, in the case of Mo-44Re (wt.%) coating, a higher concentration of rhenium silicide was observed compared to that of coating containing 15% Re. The Re-containing silicide layers were characterized by a presence of lower content of hexagonal $MoSi_2$ compared to that of non-alloyed $MoSi_2$. The oxidation resistance of both coatings containing rhenium was comparable; however, the one with a higher amount of Re exhibited slightly higher durability in high-temperature oxidation.

Keywords Mo-Re coatings · $MoSi_2$ · oxidation · siliconizing · thermal spraying

Introduction

The engineering materials dedicated to the glass industry are exposed to extremely harmful conditions, including high temperature, corrosion, oxidation, rapid temperature changes, and other factors (Ref 1, 2). The material that meets the discussed requirements is molybdenum (Ref 2, 3). The pure Mo and Mo alloys are commonly used in such elements as melting tanks, electrodes in glass melting, stirrers, stirrer cores, heating elements, and other tools in the glass pulling process (Ref 3–6). Mo exhibits numerous beneficial properties, including resistance to high temperatures (up to 1600 °C) and thermal shock, high corrosion and abrasion resistance, high modulus of elasticity, low specific heat, good wettability by the molten glass, and chemical inertness toward this medium (Ref 7–10). The last-mentioned feature is crucial for avoidance of a detrimental glass coloring, which is an effect of permeation of ions toward the glass (Ref 11). The discussed properties make Mo alloys the most reliable materials dedicated to the glass industry. Mo and its alloys ale are also utilized in the nuclear power industry (Ref 12).

A substantial disadvantage of the molybdenum alloys is high price (Ref 13). Therefore, the authors proposed a new concept of refractory products (Ref 14). This solution offers usage of other high-temperature materials (e.g., ceramic–metal composites) covered with Mo-based coatings. The deposition of such coatings allows to maintain

✉ Grzegorz Moskal
grzegorz.moskal@polsl.pl

Damian Migas
damian.migas@polsl.pl

[1] Institute of Materials Engineering, Silesian University of Technology, Krasińskiego 8, 40-019 Katowice, Poland

[2] Institute of Non-Ferrous Metals, Sowińskiego 5, 44-100 Gliwice, Poland

beneficial properties attributed to molybdenum and reduce the cost of specialist tools for glass processing. One disadvantage of Mo alloys is a brittleness occurring after recrystallization (Ref 15, 16). This phenomenon may be impeded by rhenium addition. This refractory element also increases strength (Ref 17), ductility (Ref 17, 18) and may lower the temperature of ductile-to-brittle transition in molybdenum alloys (Ref 17–22). Moreover, rhenium increases the recrystallization temperature of Mo alloys (Ref 18) and controls the recrystallization embrittlement. Therefore, in the case of glass industry applications, the utilization of ceramic-based materials with Mo-Re coatings may significantly improve the lifetime of the components which were being made from pure Mo so far. The following solution was proposed in other publications (Ref 14, 23). Unfortunately, there is one more factor limiting the efficiency of Mo and the Mo-Re coatings in the glass industry.

This limitation which lowers the potential of these materials in glass industry applications is a very low oxidation resistance (Ref 24, 25). This factor causes a low lifetime of the tools working under extreme conditions. Above 700 °C, Mo oxidizes to the MoO_3 volatile oxide (Ref 26–28); therefore, the usage of Mo requires the deposition of oxidative resistant coatings or performance of additional surface treatment processes. However, the occurrence of other elements on the tool–glass interface and their diffusion may be unfavorable for the glass color. Therefore, the authors proposed the siliconizing process to improve the oxidation resistance of the novel Mo-based coatings. Except for the enhanced resistance to high-temperature oxidation, this solution also leads to the increase in abrasion resistance that is important in terms of wear of the glass pulling tools and other components. The discussed improvement may be achieved owing to the formation of $MoSi_2$ phase that exhibits excellent wear resistance and oxidation resistance up to a temperature of 1700 °C (Ref 29, 30). The excellent oxidation behavior of this phase is resulting from the formation of a self-healing SiO_2 layer protecting the substrate material from oxidation and corrosion at high temperatures (Ref 31). Moreover, silicon is the main element of glass; therefore, the Si-rich coatings are inert in the case of the contact with molten glass in contrary to the coatings containing other elements.

In this study, the Mo-Re coatings with different contents of Re (respectively, 15 and 44 wt.%) were deposited on the ZrO_2-Mo composite by the hybrid process composed of atmospheric plasma spraying and pack siliconizing. The paper aims to characterize the structure and properties of the novel Mo-Re coatings obtained in the discussed hybrid process, which was used as a method leading to the oxidation resistance enhancement. The characterization includes an analysis of starting materials, evaluation of the morphology, chemical, and phase composition of the successfully obtained Si-rich coatings. Moreover, the examination of their durability in terms of high-temperature oxidation was carried out.

Experimental Procedure

The Starting Powders

Powders with compositions Mo-15Re and Mo-44Re (wt.%), used to deposition of the novel heat-resistant coatings, were synthesized via powder metallurgy route. The precursor materials for the powders' obtainment were ammonium perrhenate powder of 99.99% purity (a source of Re) and Mo metal powder (over 99% purity). The process of synthesis was based on reduction and high-temperature operations. The detailed description of the synthesis is shown in the other publication (Ref 14).

Deposition of the Mo-Based Coatings and Siliconizing

Cuboidal specimens of size 6 × 2 × 1 cm used in this investigation were made of the ZrO_2-Mo composite. The obtained metallic powders were thermally sprayed on the substrate of specimens. The coatings were deposited via the atmospheric plasma spraying (APS) process. The detailed parameters of adequate thermal spraying deposition are available in the other publication (Ref 14).

The Si-enrichment of the investigated Mo-Re and Mo coatings was performed using pack siliconizing technique. The process was carried out at temperature 1050 °C for 6 h under argon protective atmosphere. The pack mixture for the coating was composed of inert filler (Al_2O_3), activator (NH_4F), and Si powder. The chemical composition of pack was $22Si\text{-}2.5NH_4F\text{-}75.5Al_2O_3$ (wt.%).

Analysis Methods

The phase identification concerning thermally sprayed TBC coatings and the specimens after hot corrosion experiments were performed by x-ray diffraction (XRD). The measurements were taken using Phillips X'Pert^3 Powder diffractometer fitted with a copper anode tube ($\lambda_{CuK\alpha}$—1.54178 Å), operating at 30 mA/40 kV. The recording was performed with a stepwise approach of 0.02° step in the range of 10–90° 2θ. Another step of powders' characterization was an evaluation of their morphology. This investigation was performed using scanning electron microscopy (SEM) by Hitachi S-3400 N, equipped with energy dispersion spectrometer (EDS, Thermo Noran

System Six). The same equipment was used for the analysis of chemical composition in microareas.

Afterward, the surface of plasma-sprayed coatings was investigated because of the morphology and chemical composition. This analysis was carried out via SEM/EDS. Moreover, the phase composition of coatings was analyzed. The SEM/EDS and x-ray diffraction methods were also used in the case of the characterization of coatings after the siliconizing process. In this case, both plan-view and cross-sectional observations were performed.

The last part of the study concerned oxidation experiments. The coated specimens were exposed to the oxidation at different temperatures (1000, 1100 and 1200 °C) in a furnace atmosphere. The time of each oxidation was 25 h; the exposure time was adequate to the single life cycle of the most loaded Mo components dedicated to the glass melting applications. The specimens were heated and cooled with a furnace to exposition and room temperature, respectively. The overall condition of the oxidized samples was evaluated. Potential durability of proposed refractory products was evaluated as an effect of these investigations. Moreover, the SEM/EDS analysis, the oxidized surfaces, was performed in order to investigate the type of oxidation products.

Results and Discussion

Characterization of Powders Used to Coatings Deposition

Figures 1(a), (b) and (c)shows the phase composition of pure Mo, Mo-15 Re, and Mo-44 (wt.%) feedstock powders. In all cases, the diffraction peaks showed the occurrence of Mo with the cubic crystal structure (ICDD No. 42-1120) and additionally Re with hexagonal structure (ICDD 42-1120) in the case of modified powders. For Mo-44Re (wt.%) powder (Fig. 1c), a substantial increase in the intensity of the peaks corresponding to Re was observed in comparison to that of Mo-15Re (wt.%) powder (Fig. 1b). This observation is in accordance with the expectations. Moreover, taking into account the phase composition, the x-ray diffraction patterns confirmed relatively high quality of the powder materials used in the investigation.

The morphology and chemical composition of utilized feedstock powders are shown in Fig. 2 and 3. The pure Mo powder is a commercial material and was not analyzed (Fig. 2a, b). In the case of Mo-15Re (wt.%) powder (Fig. 3a, b), some impurities (Mg, Ca, Fe) were noticed. Moreover, the content of Re is higher compared to that of the nominal composition. A similar conclusion may be drawn after the chemical composition analysis of Mo-44 Re (wt.%) powder (Fig. 3c, d). In this case, the weight

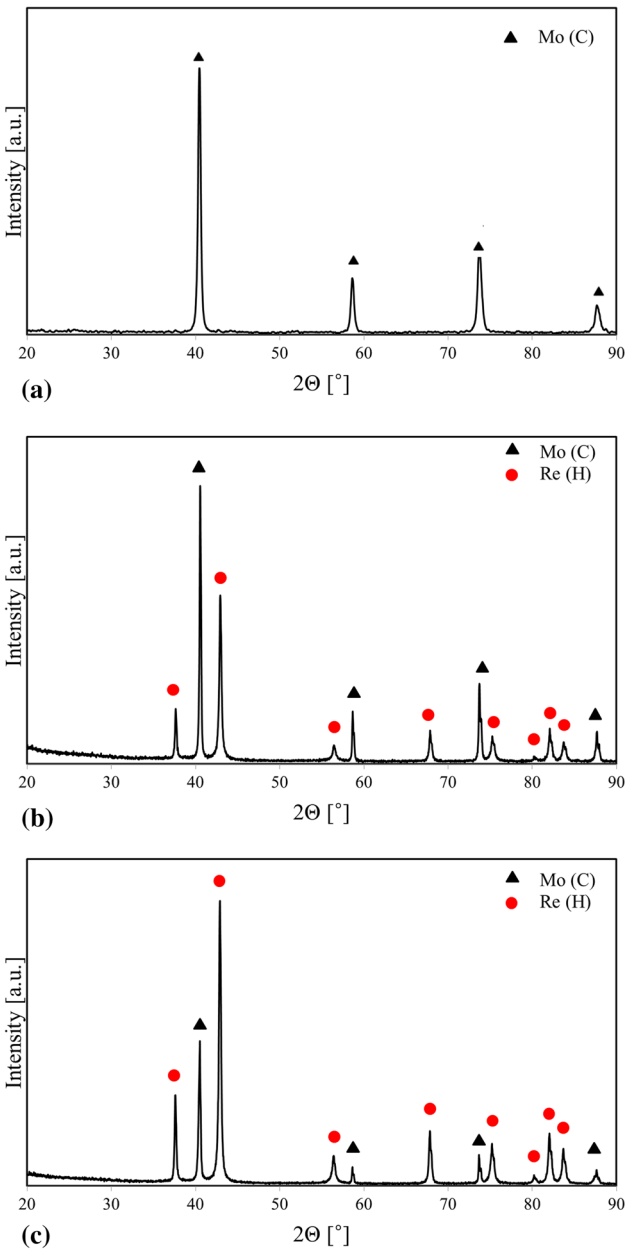

Fig. 1 XRD patterns showing phase composition of starting powders: (a) Mo; (b) Mo-15Re; (c) Mo-44Re

content of Re was about 20% higher related to that of nominal composition. This observation implies that the Mo-Re powders may be slightly inhomogeneous. In the case of Mo-44Re (wt.%) powder, the occurrence of Fe was also detected. The presence of impurities may be a result of both specimen preparation and powders' synthesis. The morphology of powders' particles is oval in both cases, which is beneficial because of thermal spraying.

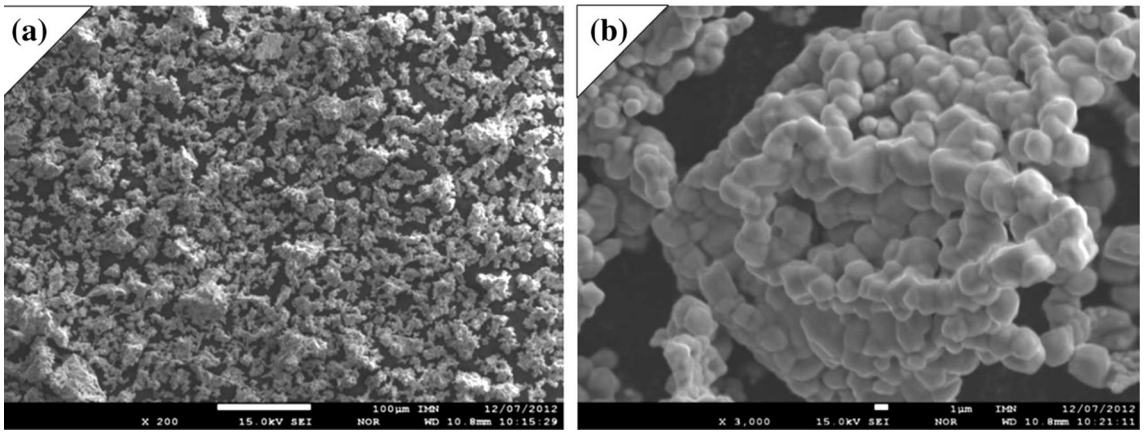

Fig. 2 Morphology of starting Mo powder used for coatings deposition

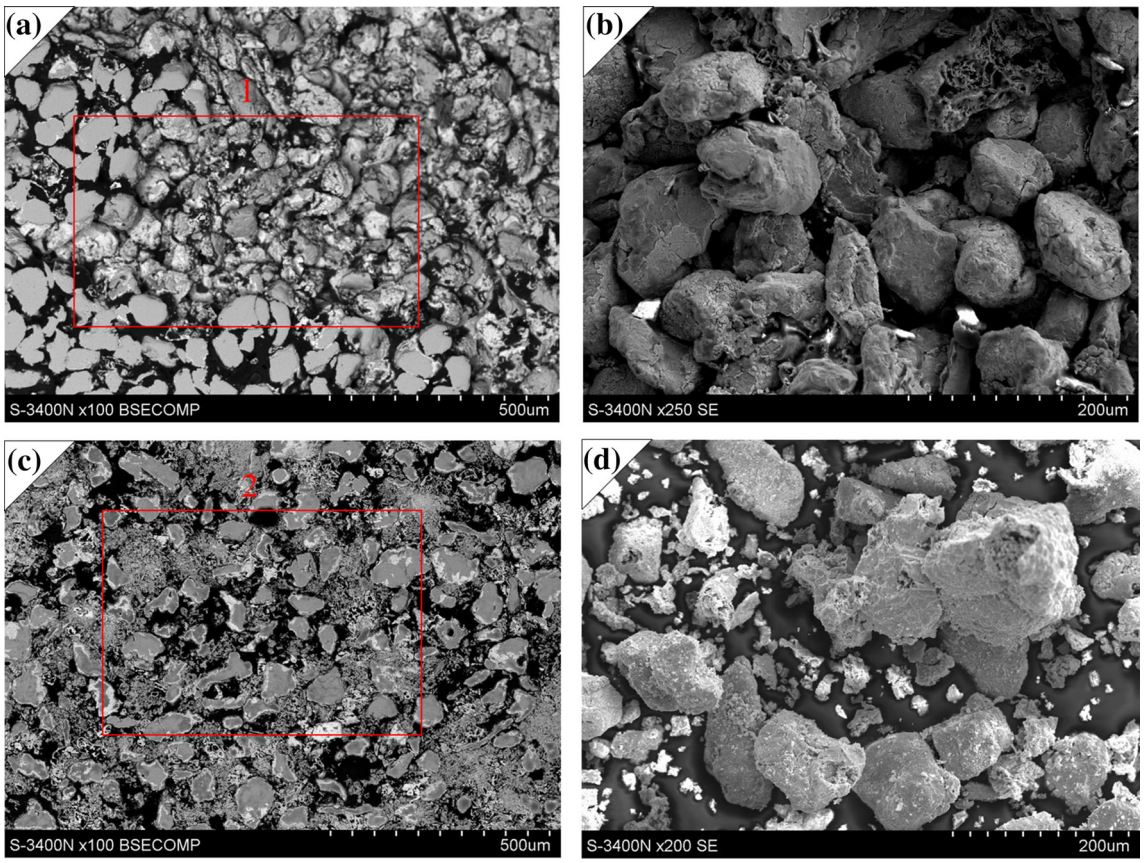

Chemical composition measured in micro areas marked above

Atom %	Mg	Ca	Fe	Mo	Re	Weight %	Mg	Ca	Fe	Mo	Re
Area 1	1.7	2.5	1.5	69.4	24.9	Area 1	0.4	0.9	0.7	57.8	40.2
Area 2	-	-	3.5	51.3	45.2	Area 2	-	-	1.5	36.3	62.2

Fig. 3 Morphology of starting powders used for coatings deposition: (a-b) Mo-15Re; (c-d) Mo-44Re

Characterization of Plasma-Sprayed Coatings

The phase composition of plasma-sprayed coatings is shown in Fig. 4. In the case of a coating composed of pure Mo, the XRD pattern (Fig. 4a) showed the occurrence of only cubic molybdenum that is in line with the expectations. Molybdenum was also the dominant phase in the case of Mo-15Re (wt.%) coating (Fig. 4b). The XRD

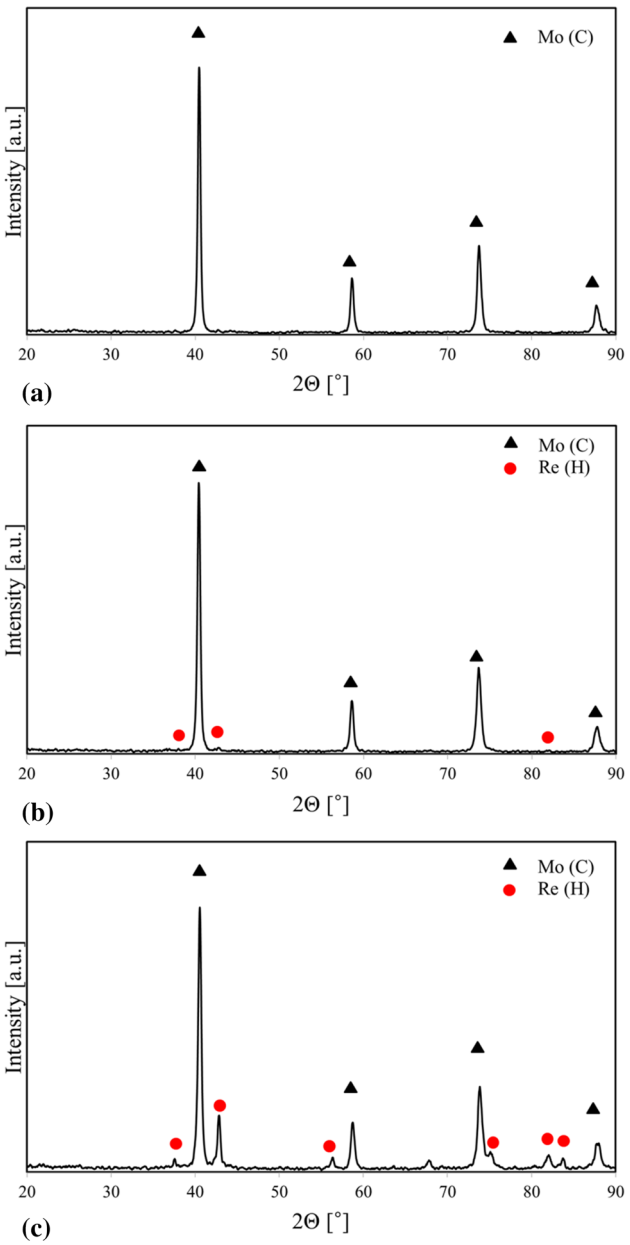

Fig. 4 XRD patterns showing phase composition of the plasma-sprayed coatings: (a) Mo coating; (b) Mo-15Re coating; (c) Mo-44Re coating

pattern corresponding to discussed coating showed some low-intense peaks corresponding to Re with hexagonal structure. In the case of Mo-44Re (wt.%) coating, molybdenum was the dominant phase, similar to that of the previous coating. However, accordingly to the chemical composition, several peaks corresponding to Re was higher compared to that of the coating containing 15% of rhenium (Fig. 4c).

The macrographs and SEM micrographs showing the surface of investigated coatings are shown in Fig. 5. In all cases, the surface topography was rough and uneven. The massive open pores were observable in the case of each coating. For the Re-containing coating, bright areas may be seen on the surface. According to BSE imaging, these places are characterized by a higher concentration of elements with a high atomic number. In this case, the brighter zones are rich in Re. Taking into account the chemical composition (Table 1), the measured content of Mo and Re in the coating is closer to the nominal one in comparison to that of the initial powder. Moreover, no impurities were detected. The differences between chemical composition on the surface of coatings and the nominal composition may imply that also in the case of deposited coating, some segregation of Re occurred. It may be better visible in the distribution of elements (Fig. 6). This figure shows the bright areas observed in Fig. 5 were mainly composed of Re. However, Mo may also be observable in this area. In other zones, the dominant element was molybdenum. However, rhenium was also present. This phenomenon indicates that the phases detected via XRD may be the solid solutions. The presence of Re in Mo and vice versa is possible due to a mutual solubility of these elements, whereas this solubility is limited (Ref 32).

Characterization of Siliconized Mo-Based Coatings

The phase composition of siliconized Mo-based coatings is shown in Fig. 7. For Mo coating subjected to the pack siliconizing (Fig. 7a), the dominant recognized phase was $MoSi_2$ with tetragonal $C11_b$ type of structure (ICDD No. 41-0612). This phase is desirable, taking into account the high-temperature performance. The second phase, characterized by the lower intensity of peaks, was also molybdenum silicide, however, characterized by hexagonal C40 type of structure (ICDD No. 81-0167). Moreover, within the Mo coating, some amount of tetragonal Mo_5Si_3 phase was detected (ICDD 34-0371). The stoichiometry of this compound implies that the detected phase may be located in some interdiffusion zone (IDZ). The occurrence of Mo_5Si_3 phase in such IDZ was reported in the case of $MoSi_2$ deposited coating on Mo substrate (Ref 33). In the case of Mo-15Re (wt.%) coating after siliconizing (Fig. 7b), tetragonal $MoSi_2$ was the dominant phase, similar to that of the previous example. The hexagonal $MoSi_2$, as well as tetragonal Mo_5Si_3 phases, were also detected; however, the intensity of peaks corresponding to those phases was substantially lower compared to that of the silicide layer on pure Mo. Moreover, a more detailed observation of the peaks allows noticing additional low-intensity peaks, placed slightly to the right from the peaks corresponding to tetragonal $MoSi_2$. Red circles mark these peaks. The discussed reflexes are corresponding to $ReSi_2$ phase with the orthorhombic structure (ICDD No. 35-1384). Although the XRD patterns showed the presence

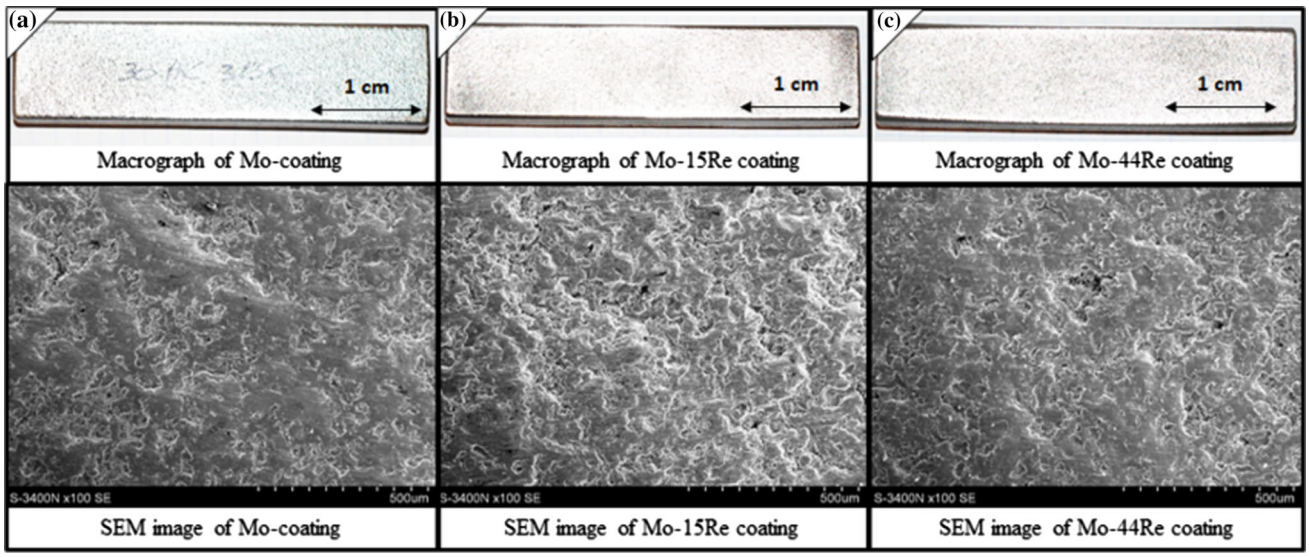

Fig. 5 Surface condition of plasma-sprayed coatings: (a) Mo coating; (b) Mo-15Re coating; (c) Mo-44Re coating

Table 1 Chemical composition from surface areas visible on Fig. 5

Type of coating	Atom%		Weight%	
	Mo	Re	Mo	Re
Mo coating	100	…	100	…
Mo-15Re coating	88.8	11.2	80.3	19.7
Mo-44Re coating	78.4	21.6	65.2	34.8

of $ReSi_2$, based on the literature data (Ref 34, 35), it was found that the stoichiometry of the rhenium silicide should be $ReSi_{1.75}$, not $ReSi_2$. The rhenium silicide was also detected in the case of siliconized Mo-44Re (wt.%) coating (Fig. 7c). However, for the last coating, the peaks corresponding to this phase were considerably more intense. The level of hexagonal $MoSi_2$ and tetragonal Mo_5Si_3 was marginal. The dominant phase was t-$MoSi_2$. The following analysis showed that the siliconizing process was performed successfully from the phase composition point of view. The surface layer rich in $MoSi_2$ phase was obtained, whereas the amount of t-Mo_5Si_3 and h-$MoSi_2$ was minimal, especially in the case of coatings containing rhenium. This phenomenon may be connected with a possible stabilization of the tetragonal $C11_b$ structure by rhenium. While V, Cr, Nb, Ta, and Al form silicides with the C40 type of structure and alloying with these elements stabilizes such type of the structure in $MoSi_2$ (Ref 36), tungsten and rhenium silicides are characterized by $C11_b$ structure. Thereby, both W and Re can be substituted for Mo in $MoSi_2$ (Ref 35). At lower temperatures, the more stable phase is $MoSi_2$ with hexagonal structure. However, at a temperature higher than 900 °C, normally, the tetragonal form of molybdenum silicide can be observed (Ref 37). In the case of coatings preparation, the temperature of the siliconizing process was 1050 °C; therefore, the presence of a tetragonal type of lattice was expected. The occurrence of hexagonal $MoSi_2$ in the siliconized Mo coating may be caused by the insufficient time of the annealing at 1050 °C; hence, t-ZrO_2 was not obtained within the entire siliconized layer. However, in the case of Re-containing coatings, the amount of the tetragonal phase was substantially lower. Thereby, the phase composition (Fig. 6b and c) should exhibit the presence of (Mo, Re)Si_2 phase. $(Mo_xRe_{1-x})Si_2$ phases form solid solutions with the $MoSi_2$, but presumably, there must be a transition from the $C11_b$ structure of $MoSi_2$ to the distorted structure of $ReSi_{1.75}$ (Ref 38). Moreover, Mo may substitute for Re in rhenium silicide (Ref 39). These effects confirm the diffusional processes between molybdenum and rhenium silicides (Ref 35).

Figure 8 shows the macrographs and SEM micrographs showing the surface of investigated coatings after the siliconizing process. The surface condition of all siliconized coatings was comparable. The surfaces were characterized by substantial roughness and the occurrence of numerous massive open pores. Taking into account, the chemical composition measured in the discussed external surfaces (Tab. 2), the composition of Mo-Re coatings is corresponding to the phase composition analysis which showed the occurrence molybdenum and rhenium silicides. In the case of Mo coating after the pack siliconizing, the amount of Si was over 80 at.% that is not corresponding to the $MoSi_2$ stoichiometry. However, the exceptionally high concentration of silicon on the surface may be an effect of Si-gradient in the coating. This effect was observed in the

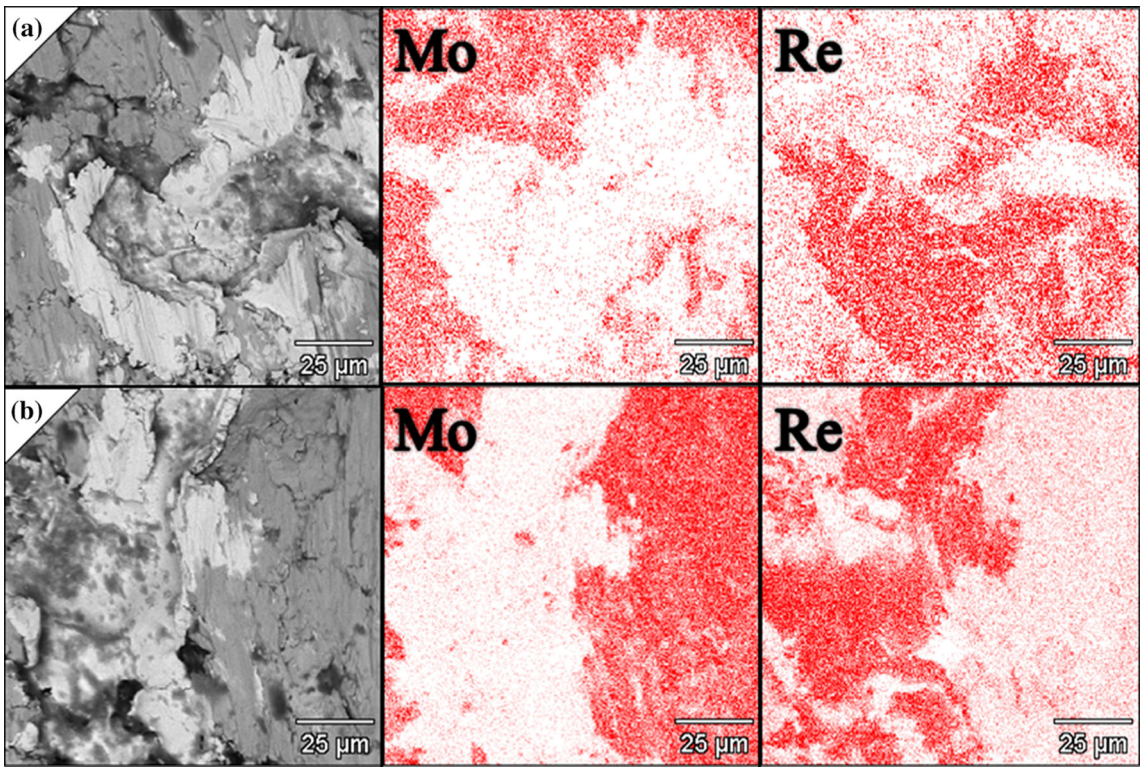

Fig. 6 Distribution of elements on the surface of plasma-sprayed coatings: (a) Mo-15Re coating; (b) Mo-44Re coating

further part of the investigation. On the surface of Mo-44Re (wt.%) coating, some impurities were observed. These elements may be a residue after the siliconizing process. In the case of all investigated surfaces, a small amount of Al was detected. The presence of this element may be connected with the utilization of the Al_2O_3 filler in the pack siliconizing method. Furthermore, Re was detected within the siliconized layer that may be corresponding to the occurrence of Mo-Re silicides.

The SEM/EDS analysis of the microstructure of Mo coating after the siliconizing process is shown in Fig. 9. The cross sections showed the presence of three different zones that are indicated by the color contrast connected with the differences in the atomic number. Due to the discussed color contrast between the zones, it can be concluded that the outer one is characterized by the dominance of elements with lower atomic number. It is in accordance with the chemical composition in microareas. The layer marked by No. 1 and No. 2 contains mainly silicon that is corresponding to the siliconized coating. This rough layer is characterized by numerous massive pores and the occurrence of cracks. In the area near the surface (marked by No. 1), the concentration of silicon is the highest (almost 75 at.%). However, the microarea marked by No. 2, which is located deeper showed the higher content of Mo (about 36 at.%) and the lower Si-content (64 at.%). This observation is other than data obtained for the area near the surface. The gradient in Si-concentration is in accordance with a diffusion character of the siliconizing process. Moreover, the chemical composition in microareas is in accordance with the analysis of phase composition (Fig. 7) that showed the different types of molybdenum silicides (mainly t-$MoSi_2$) might occur in the gradient coating. Lower the discussed layer exists the brighter the area is, which is composed of pure Mo. The chemical composition in this area implies that the present layer was Mo coating deposited by the APS method; however, the layer was located too deep to be enriched in silicon during the pack siliconizing. The morphology of the discussed layer implies that the coating was deposited via thermal spraying. This suggestion is based on the occurrence of elongated splats that form a curved lamellar structure, typical of spray coatings (Ref 40). Between the outer and Mo-rich zone exists some thin layer, which is the interdiffusion zone (Fig. 9b). The occurrence of such a layer was reported (Ref 33) and maybe corresponding to the detection of Mo_5Si_3. The presence of such zones confirms the gradient character of the obtained coating. The area marked by No. 4 showed the microstructure of the substrate composite material. This material is mainly composed of Zr; however, it also contains a considerable amount of Mo.

The similar character of the cross-sectional microstructure was observed in the case of siliconized Mo-15Re (wt.%) coating (Fig. 10). The chemical composition of the

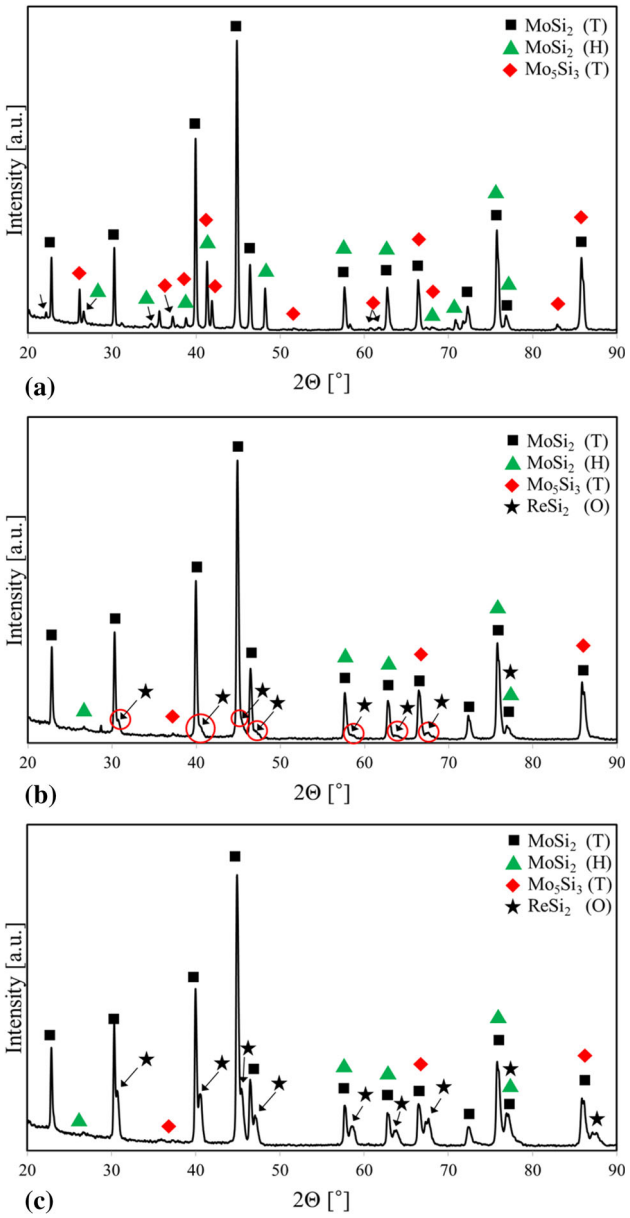

Fig. 7 XRD patterns showing phase composition of the plasma-sprayed coatings after siliconizing: (a) Mo coating; (b) Mo-15Re coating; (c) Mo-44Re coating

outer layer (Area No. 1) suggests the occurrence of silicide coating that was confirmed by XRD analysis. Moreover, some amount of Re (1.5 at.%) was observed. The presence of Re in the discussed layer may be connected with the occurrence of (Mo, Re)Si_2 and $ReSi_{1.75}$ phases, whose existence was implied in the phase composition analysis. A zone characterized by the dominant content of Mo was observed below the siliconized layer. A similar effect was found for Mo coating. The chemical composition of the discussed layer is to some extent corresponding to the Mo-Re alloy with the lower concentration of rhenium. However, in this case, some bright areas were observed in both Mo-Re coating and Si-rich layer (marked by Point No. 4). These areas are composed of rhenium and imply that some segregation of this element occurred within the Mo-Re layer. The same areas were observed in the siliconized layer (marked by red circles). Moreover, in Mo-Re zone, the areas characterized by roughly 40 wt.% of Re were observed (Point No. 5). In the other places of the discussed layer (marked by Area No. 3), the content of Re did not exceed 5 wt.%.

The microstructure of siliconized Mo-44Re (wt.%) coating is shown in Fig. 11. In this case, the chemical composition of the external layer was also in accordance with the phase analysis; however, the twice higher amount of Re was detected compared to that of the silicide layer of the Mo-15Re (wt.%) coating. This layer was also characterized by the substantial surface roughness and occurrence of some bright areas, mostly composed of rhenium (Point No. 4). These areas were also observed in Fig. 10. The morphology of the middle layer was analogous to that of Mo-15Re (wt.%) alloy; however, the discussed layer was characterized by a higher amount of Re. In the case of Mo-15Re and Mo-44 Re (wt.%) coatings, the interdiffusion zone may also occur due to the presence of Mo_5Si_3; however, this layer could be very thin. The considerably low thickness of this zone may be corresponding to the minimal amount of Mo_5Si_3 phase, shown by the XRD patterns. The comparison of linear distributions of essential elements such as Mo, Si, and Re for all types of coatings is shown in Fig. 12. This analysis confirmed the observations from the EDS characterization of Mo and Mo-Re coatings in microareas after siliconizing process.

High-Temperature Oxidation of Siliconized Mo-Based Coatings

The macrographs of siliconized Mo, Mo-15Re and Mo-44Re (wt.%) coatings after high-temperature oxidation tests are shown in Fig. 13. Products of oxidation covered all coatings after 25 h of oxidation at 1000 °C; however, the overall condition of the surfaces was satisfactory. No substantial cracks or other volume defects were observed except siliconized Mo coating. Additionally, in the case of Mo-44Re (wt.%) coating, some spallation of the oxide layer was found. After oxidation at temperature 1100 °C, some longitudinal cracks were observed in the case of Mo and Mo-15Re (wt.%) siliconized coatings. The condition of the Mo-44Re (wt.%) specimen was similar compared to that of after oxidation at 1000 °C. In the case of oxidation at 1200 °C, both Mo-Re specimens were substantially cracked after cooling to room temperature. The sample based on pure molybdenum after siliconizing was destroyed at this temperature. This failure implies that 25 h

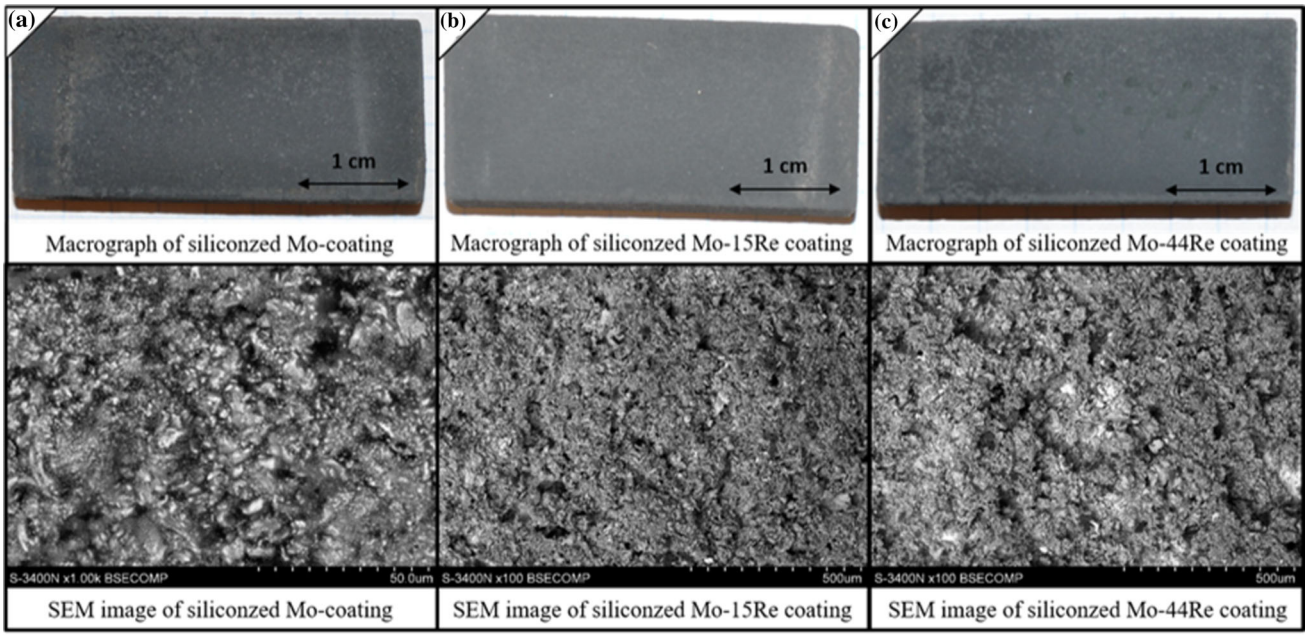

Chemical composition in micro areas measured on siliconized surfaces

Type of coating	Atom %					
	Al.	Si	Cl	Ca	Mo	Re
Mo coating	0.4	82	-	-	17.6	-
Mo-15Re coating	0.3	66.2	-	-	29.7	3.8
Mo-44Re coating	1.1	62.1	1.9	1.8	26.7	6.4
Type of coating	Weight %					
	Al.	Si	Cl	Ca	Mo	Re
Mo coating	0.3	57.5	-	-	42.2	-
Mo-15Re coating	0.2	34.2	-	-	52.5	13.1
Mo-44Re coating	0.5	30.8	1.2	1.3	45.2	21

Fig. 8 Surface condition of plasma-sprayed coatings after siliconizing: (a) Mo coating; (b) Mo-15Re coating; (c) Mo-44Re coating

Table 2 Chemical composition from surface areas visible on Fig. 8

Type of coating	Atom%					
	Al	Si	Cl	Ca	Mo	Re
Mo coating	0.4	82	…	…	17.6	…
Mo-15Re coating	0.3	66.2	…	…	29.7	3.8
Mo-44Re coating	1.1	62.1	1.9	1.8	26.7	6.4
Type of coating	Weight%					
	Al	Si	Cl	Ca	Mo	Re
Mo coating	0.3	57.5	…	…	42.2	…
Mo-15Re coating	0.2	34.2	…	…	52.5	13.1
Mo-44Re coating	0.5	30.8	1.2	1.3	45.2	21

of oxidation at this temperature was enough to wear out the siliconized Mo coatings.

These results imply that Mo-15Re (wt.%) coating may withstand 25 h of oxidation at 1100 °C, whereas after oxidation at 1100 °C, substantial cracks occurred on the surface. In the case of Mo-44Re (wt.%) coating, oxidation at both 1000 and 1100 °C did not lead to considerable failure of the external layer. It should be noted that the substantial destruction of the specimens oxidized at 1200 °C may be too great extent caused by cooling that generates the tensile stress. In the case of glass processing, the protective layer is subjected to compressive stresses that are more favorable for coatings.

The macrograph (Fig. 14a) shows a color diversity within the oxidized surface for Mo-15Re specimen after siliconizing process and oxidation at temperature 1000 °C. This kind of surface appearance may imply a different character of the oxidation products. The SEM/EDS analysis showed the presence of various oxides in view of chemical composition and morphology. The dominant type of the external layer observed via scanning electron

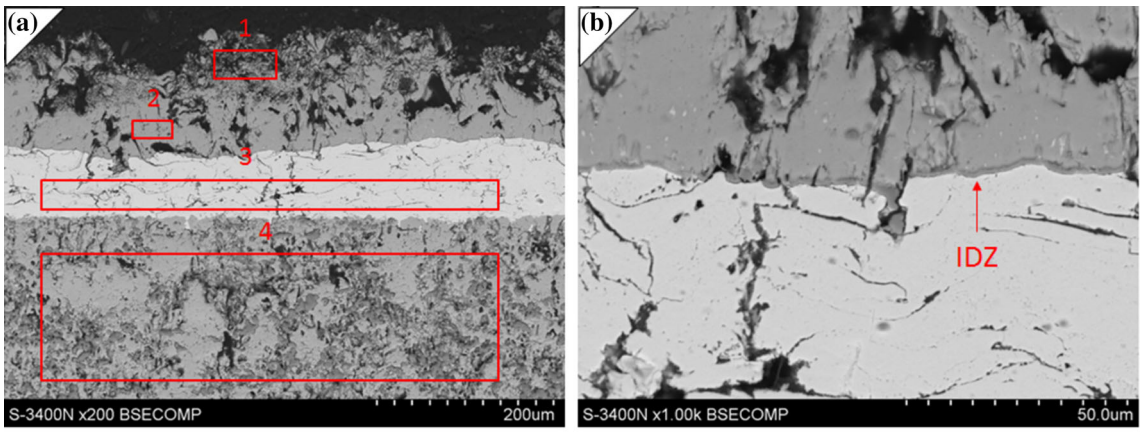

Chemical composition measured in micro areas marked above

Atom %	Mg	Al	Si	Zr	Mo	Weight %	Mg	Al	Si	Zr	Mo
Area 1	-	-	74.7	-	25.3	Area 1	-	-	46.3	-	53.7
Area 2	-	-	63.7	-	36.3	Area 2	-	-	33.9	-	66.1
Area 3	-	-	-	-	100	Area 3	-	-	-	-	100
Area 4	1.5	2.7	12.2	60	23.6	Area 4	0.4	0.9	4.2	66.9	27.6

Fig. 9 SEM/EDS analysis of the cross section of siliconized Mo coating

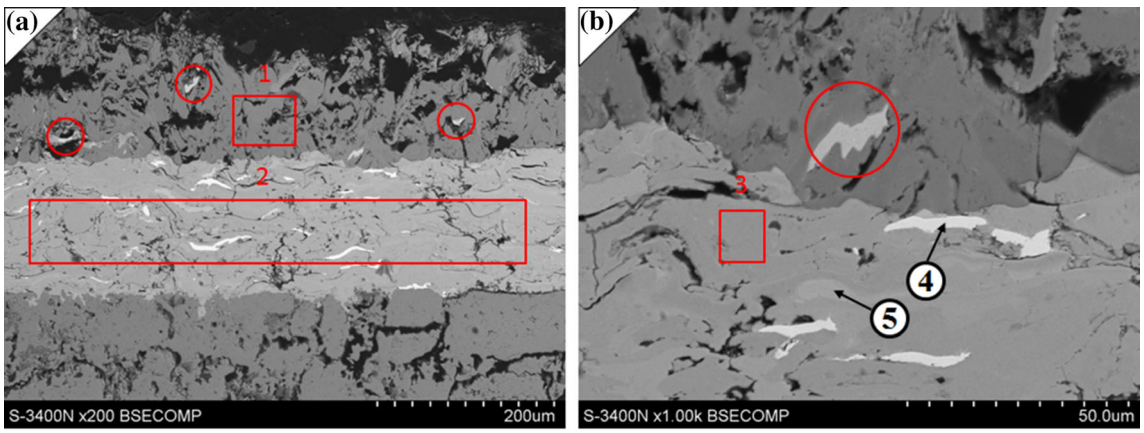

Chemical composition measured in micro areas marked above

Atom %	Al	Si	Mo	Re	Weight %	Al	Si	Mo	Re
Area 1	0.9	63	34.6	1.5	Area 1	0.5	32.8	61.5	5.2
Area 2	-	-	94.4	5.6	Area 2	-	-	89.6	10.4
Area 3	-	-	97.4	2.6	Area 3	-	-	95.1	4.9
Point 4	-	-	-	100	Point 4	-	-	-	100
Point 5	-	-	74.8	25.2	Point 5	-	-	60.4	39.6

Fig. 10 SEM/EDS analysis of the cross section of siliconized Mo-15Re coating

microscopy (SEM) is an area marked with No. 2 (Fig. 14c). The presence of ca 95 at.% of silicon characterizes this place. The high Si-content suggests that on the top surface, the dominant oxide was SiO_2. This type of oxide is a typical product of oxidation in the case of silicide-based materials (Ref 41, 42). Moreover, within the investigated surface, numerous oxide particles enriched in Zr were observed (Area No. 1 and Point Nos. 3, 9). Furthermore, Al-rich oxides were also found (Point Nos. 5, 9). The surface of the oxidized specimen is mainly composed of Si that may be corresponding to the occurrence of SiO_2. Moreover, on the surface, much content of Al, Mo, and Zr was noticed in some places. The Al-oxides are present on the scale due to the occurrence of Al in the coating after siliconizing. Zr is the main element of the cermet, whereas Mo is present in both the coating and the substrate. In the case of all investigated areas and points, oxygen was also present; however, this element can not be quantitatively detected via the EDS method.

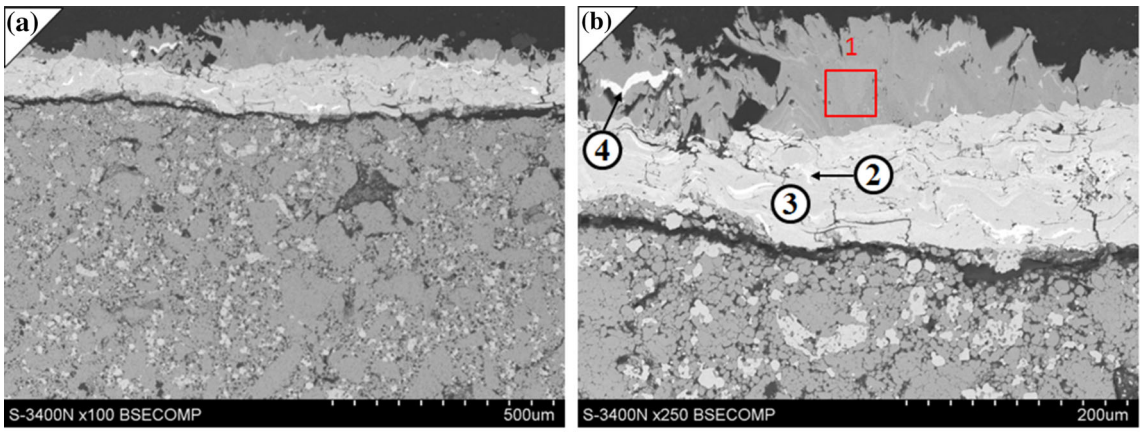

Chemical composition measured in micro areas marked above

Atom %	Si	Zr	Mo	Re	Weight %	Si	Zr	Mo	Re
Area 1	59.4	-	37.6	3	Area 1	28.6	-	61.9	9.5
Point 2	-	-	87.4	12.6	Point 2	-	-	78.2	21.8
Point 3	-	-	94.5	5.5	Point 3	-	-	89.9	10.1
Point 4	-	1.9	-	98.1	Point 4	-	0.9	-	99.1

Fig. 11 SEM/EDS analysis of the cross section of siliconized Mo-44Re coating

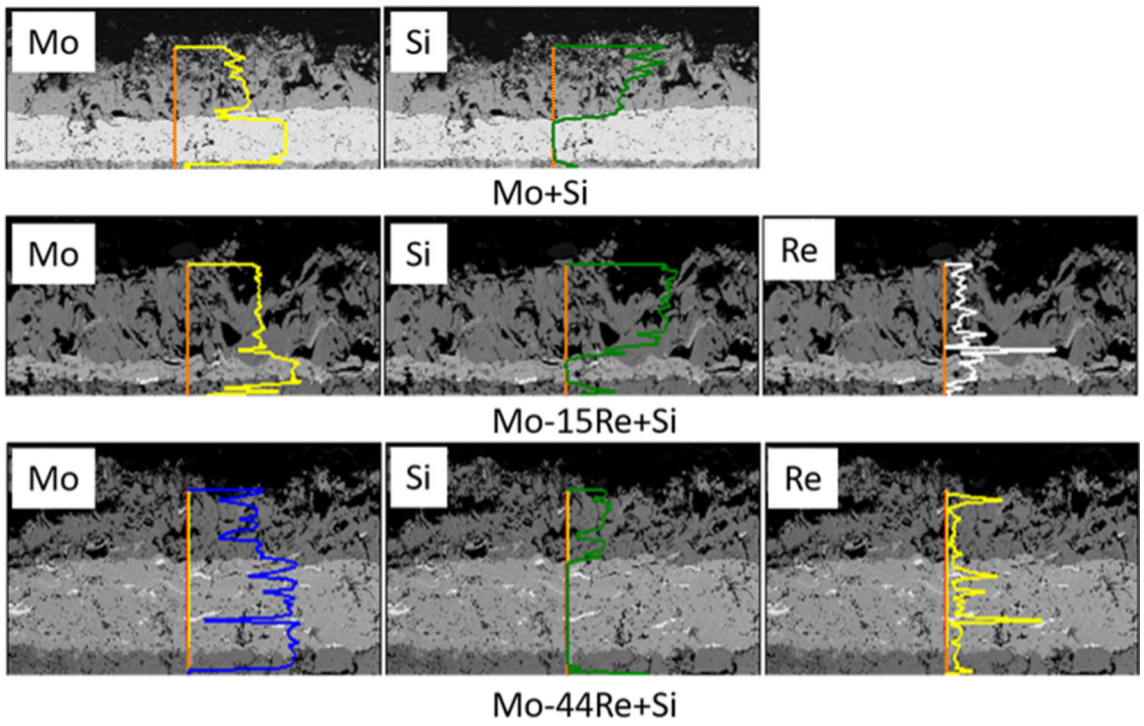

Fig. 12 Linear elements distributions in Mo and Mo-Re coatings after siliconizing process

A similar surface condition of the oxidized coating was observed in the case of another specimen (Fig. 15). However, in the case of Mo-44Re (wt.%) coating, some spallation of the external layer occurred after cooling to room temperature, thereby, two specific areas (area "A" and "B") may be observable (Fig. 15a). The zone marked by letter A is an external one, and this place is corresponding to the area marked by No. 1. In this case, the chemical composition analysis in the microarea showed the presence of roughly 85 at.% of silicon. This Si-content is similar to that of an external layer of the previous coating after oxidation (Fig. 14c, Area No. 2). The SiO_2 is believed to be the dominant phase; in this case, however, this layer also contains numerous, tiny, bright particles. These oxidation

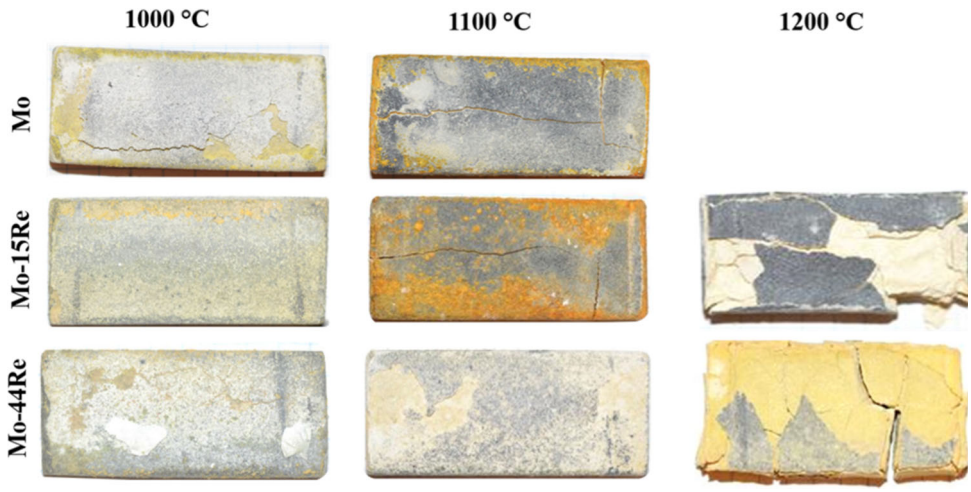

Fig. 13 Macrographs of the siliconized coatings after oxidation experiments

products are rich in Zr and Mo. The discussed zone also contains a small amount of Al and some other elements. The presence of a second characteristic zone (marked by letter B) is a result of the spallation of zone "A" after cooling. This zone contains a considerable amount of Al and Zr. The color contrast implies the occurrence of two dominant types of oxidation products. The first one is Al-rich oxide (marked by No. 7) with over 80 at.% of Al. The second one (denoted by No. 6) is rich in Zr (almost 50 at.%), however, also Al and Si were detected in this area. In the case of discussed SEM/EDS analysis, also oxygen was detected in all investigated points and areas. The various distribution of elements implies that in this zone occurred the mixture of different types of oxides. The high Al-content may mean that due to the oxidation of Al present in the siliconized coating, some Al-rich oxide layer occurred below the external Si-rich area.

Similar effects were observed in the case of Re-free reference Mo coating after the siliconizing process (Fig. 16).

In the case of Mo-15Re (wt.%) coating after oxidation tests at 1100 °C, the macrograph (Fig. 17a) shows a color diversity within the oxidized surface and occurrence of cracks. The SEM/EDS analysis showed a variety of oxidation products. The most common type of area on the discussed surface is shown in Fig. 17(c), and (d). This area was mainly composed of Si (Point No. 7); however, the discussed zone contained also such elements as Al and Zr. This composition is similar to that of specimens after oxidation at 1000 °C. The second characteristic zone is shown in Fig. 17(b), (d), and (f). This area is rich in Mo, Al, and Mg. In the case of all investigated areas and points, oxygen was also detected. The external layer oxidized layer in the case of Mo-15Re (wt.%) coating after oxidation at 1100 °C was composed of the mixture of oxides rich in Si, Mo, Al, and Mg.

Figure 18 shows the SEM/EDS analysis of the surface of siliconized Mo-44Re (wt.%) coating after oxidation at 1100 °C for 25 h. The surface condition is almost analogous to that of after oxidation of Mo-44Re (wt.%) coating at 1000 °C. Because of the surface appearance (Fig. 18a), two specific zones may be distinguished. The top layer (zone "A") and the internal layer (zone "B"), which was uncovered by the previous one due to the peeling of the scale during cooling. Taking into account the chemical composition and morphology, the first zone ("A") is the same zone, which occurred on the top in the previous cases. This layer is believed to be the external silicon dioxide layer due to the very high content of Si. The second characteristic zone (marked by letter "B") is analogous to that observed in the case of oxidation at 1000 °C (Fig. 15c-zone B). This layer is composed of the mixture of Zr-, Al-, and Si-rich oxides. Similar effects were observed in the case of Re-free Mo coating after the siliconizing process and tested at temperature 1100 °C (Fig. 19).

The specimens after oxidation at 1200 °C were cracked; therefore, their surface condition may differ from that of after oxidation at lower temperatures. For Mo-15Re (wt.%) coating, the first difference is the occurrence of a third characteristic zone (Fig. 20a-zone C), which is corresponding to the substrate. Because of chemical composition, this zone is mainly composed of Zr, which may imply this zone is near the substrate. However, in this area, no molybdenum was detected, whereas some amount of Si was present. It may suggest that the discussed zone is some oxide layer grown near the substrate. The zones marked by letters A and B are comparable to those observed in the previous cases (e.g., in Fig. 18).

Figure 21 shows the surface condition of siliconized Mo-44Re (wt.%) coating after oxidation at 1200 °C. In this case, the two specific areas may be observable on the surface. The area marked by letter A is mainly composed

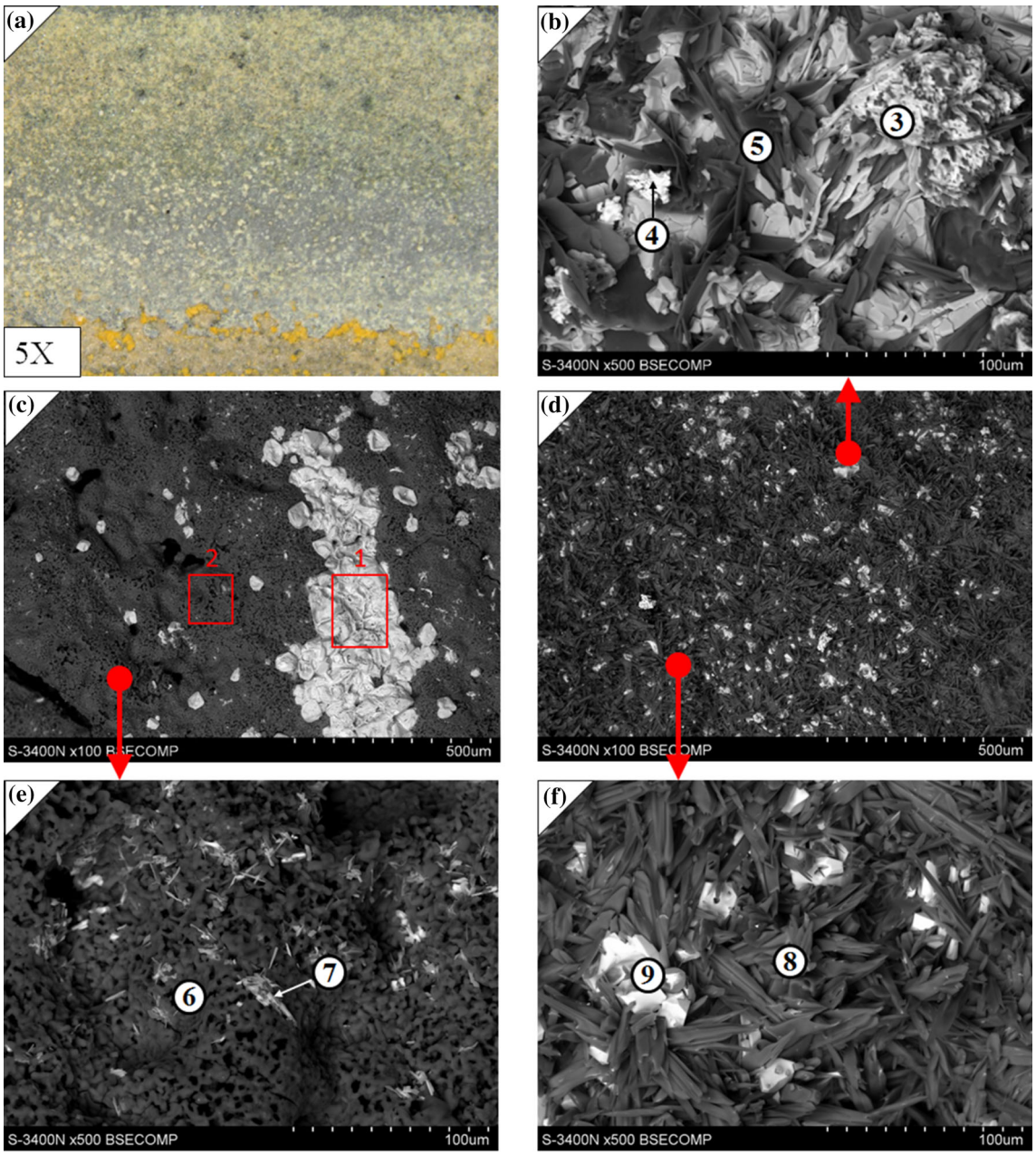

Chemical composition measured in micro areas marked above

Atom %	Al	Si	Zr	Mo	Re	Weight %	Al	Si	Zr	Mo	Re
Area 1	0.5	46.1	46.4	7	-	Area 1	0.2	20.8	68.1	10.9	-
Area 2	-	95.4	3.1	1.5	-	Area 2	-	86.2	9.1	4.7	-
Point 3	27.9	9.1	23.3	39.7	-	Point 3	10.9	3.7	30.6	54.8	-
Point 4	12.7	51.2	2	29.8	4.3	Point 4	6.1	25.6	3.2	50.8	14.3
Point 5	73.3	18.4	6.6	1.7	-	Point 5	60.8	15.9	18.4	4.9	-
Point 6	-	98.7	-	1.3	-	Point 6	-	95.6	-	4.4	-
Point 7	-	77.9	-	22.1	-	Point 7	-	50.8	-	49.2	-
Point 8	61.4	36.8	0.9	0.9	-	Point 8	58	36.1	2.9	3	-
Point 9	16	40.1	43.9	-	-	Point 9	7.8	20.2	72	-	-

Fig. 14 SEM/EDS analysis of the surface of siliconized Mo-15Re after oxidation at 1000 °C for 25 h

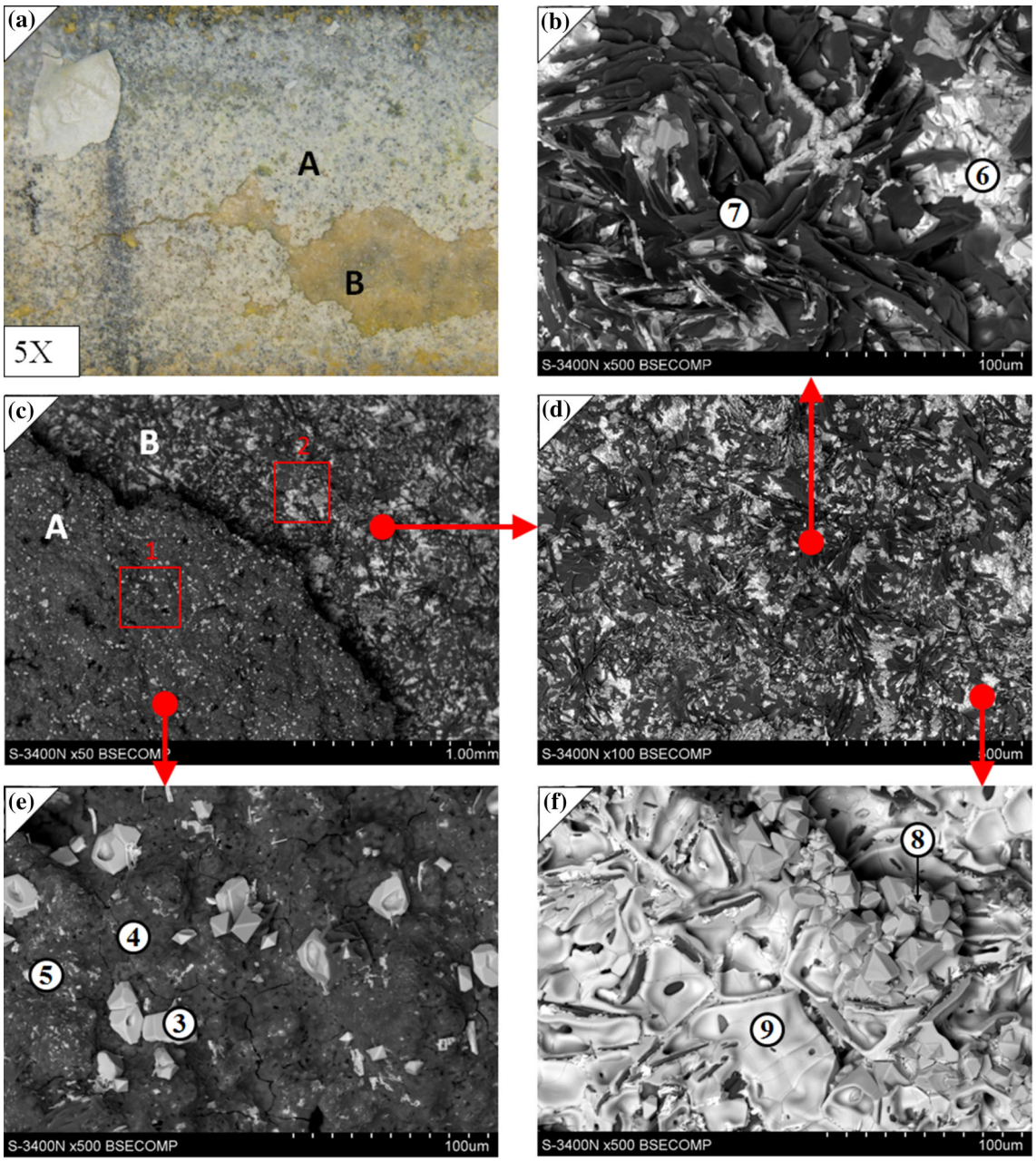

Chemical composition measured in micro areas marked above

Atom %	Mg	Al	Si	K	Ca	Fe	Zr	Mo	Weight %	Mg	Al	Si	K	Ca	Fe	Zr	Mo
Area 1	-	2.5	84.4	-	1.4	0.7	3.2	7.8	Area 1	-	1.9	66.4	-	1.6	1	8.1	21
Area 2	-	66.4	8.2	-	0.8	2.2	18.2	4.2	Area 2	-	42.4	5.4	-	0.8	2.8	39.2	9.4
Point 3	-	0.6	53.8	-	-	-	45.6		Point 3	-	0.3	26.5	-	-	-	73.2	-
Point 4	-	0.6	92.5	-	-	-	2.4	4.5	Point 4	-	0.5	79.6	-	-	-	6.8	13.1
Point 5	1.7	2	60	1.5	2.4	2.4	-	30	Point 5	0.8	1.1	34.1	1.2	1.9	2.7	-	58.2
Point 6	-	23.5	28.1	-	-	0.7	47.7		Point 6	-	10.9	13.6	-	-	0.7	74.8	-
Point 7	-	82.7	4.1	-	-	3	8.4	1.8	Point 7	-	64.6	3.3	-	-	4.9	22.2	5
Point 8	-	7.8	34.3	-	6.8	-	40.6	10.5	Point 8	-	23.5	28.1	-	-	0.7	47.7	-
Point 9	-	6.7	1.2	-	47.8	0.5	-	43.8	Point 9	-	82.7	4.1	-	-	3	8.4	1.8

Fig. 15 SEM/EDS analysis of the surface of siliconized Mo-44Re after oxidation at 1000 °C for 25 h

of Si-oxides; however, also Mg and Al were detected. The second zone was located under the first one. Due to the spallation of the external oxide layer, this area was uncovered. Within the discussed place, oxides rich in Mo,

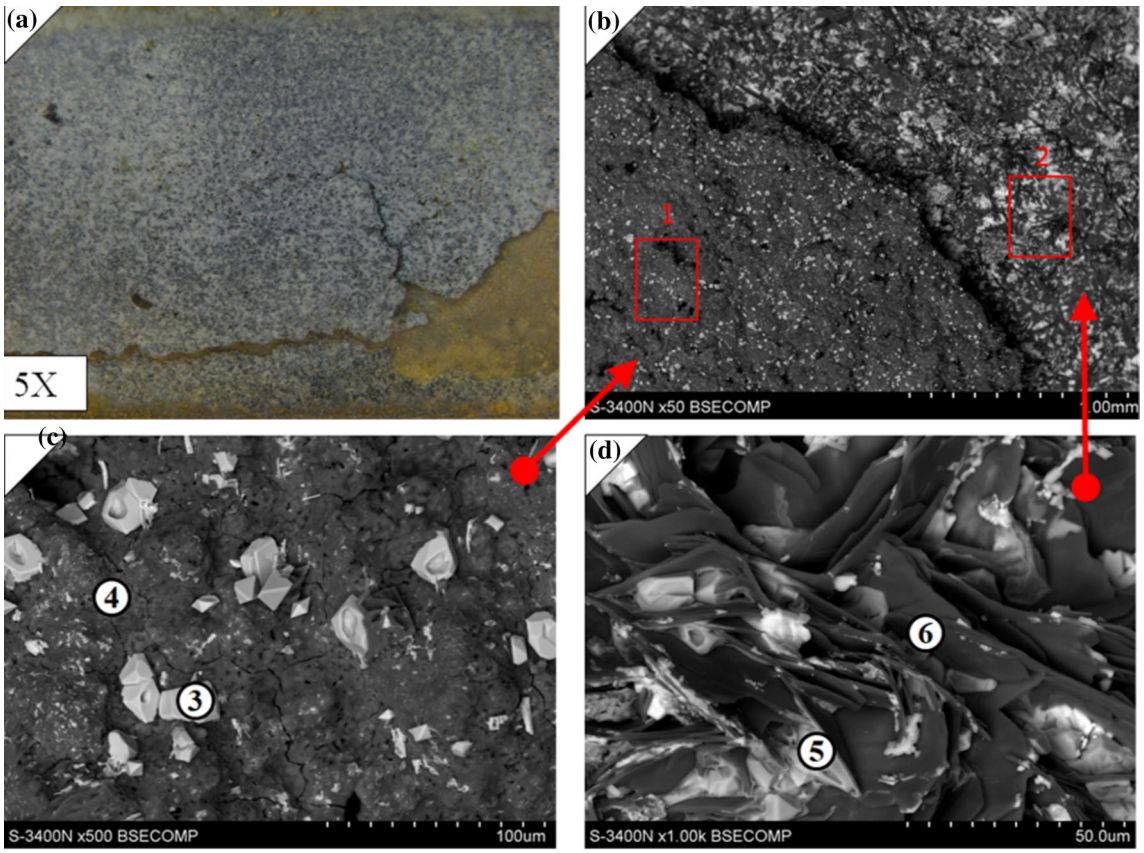

Chemical composition measured in micro areas marked above

Atom %	Al	Si	Zr	Mo	Fe	Weight %	Al	Si	Zr	Mo	Re
Area 1	2.5	84.4	3.2	9.9	-	Area 1	1.9	66.3	10.8	21.0	-
Area 2	66.5	8.3	21.2	4.2	-	Area 2	42.4	5.4	42.78	9.4	-
Point 3	0.6	53.8	45.6	-	-	Point 3	0.3	26.5	73.2	-	-
Point 4	0.6	92.5	2.4	4.5	-	Point 4	0.5	79.6	6.8	13.1	-
Point 5	23.5	28.1	48.4	-	-	Point 5	10.9	13.6	75.5	-	-
Point 6	82.7	4.1	8.4	1.8	3.0	Point 6	64.6	3.3	22.2	5.0	4.9

Fig. 16 SEM/EDS analysis of the surface of siliconized Mo after oxidation at 1000 °C for 25 h

Mg, and Si were observed. Taking into account the character of the top layer, in all cases, the same type of oxides was found. This type of external layer is probably composed of SiO_2 and a small number of other oxides. Other layers are also comparable between the different coatings and temperatures of oxidation; however, they slightly differ in chemical composition and morphology.

Summary

The two Mo-Re coatings (and Mo-based coating as reference material) were deposited on the ceramic–metal composite using a hybrid process of atmospheric plasma spraying with subsequent diffusional siliconizing in the pack. The morphology of the obtained coating was adequate to utilize the deposition technique. From the microstructural point of view, the Mo-Re coatings were comparable to those of composed of pure Mo. However, in the case of Re-containing coatings, some segregation of rhenium occurred on the surface. The Re-segregation occurred at a greater extent in the case of Mo-44Re (wt.%) coating. Subsequently, the coatings were subjected to the pack siliconizing. The microstructure of the final siliconized Mo-Re coatings was evaluated. The coatings were composed of two zones. The first one was Mo-Re layer with a characteristic splat structure. The second, upper layer was the rough, porous layer, formed of Si, Mo, and small amounts of Re. The microstructure of siliconized Mo coating was similar because of the layer structure. Between discussed characteristic layer in siliconized Mo and Mo-Re coatings, some interdiffusion zone was observed. Based on

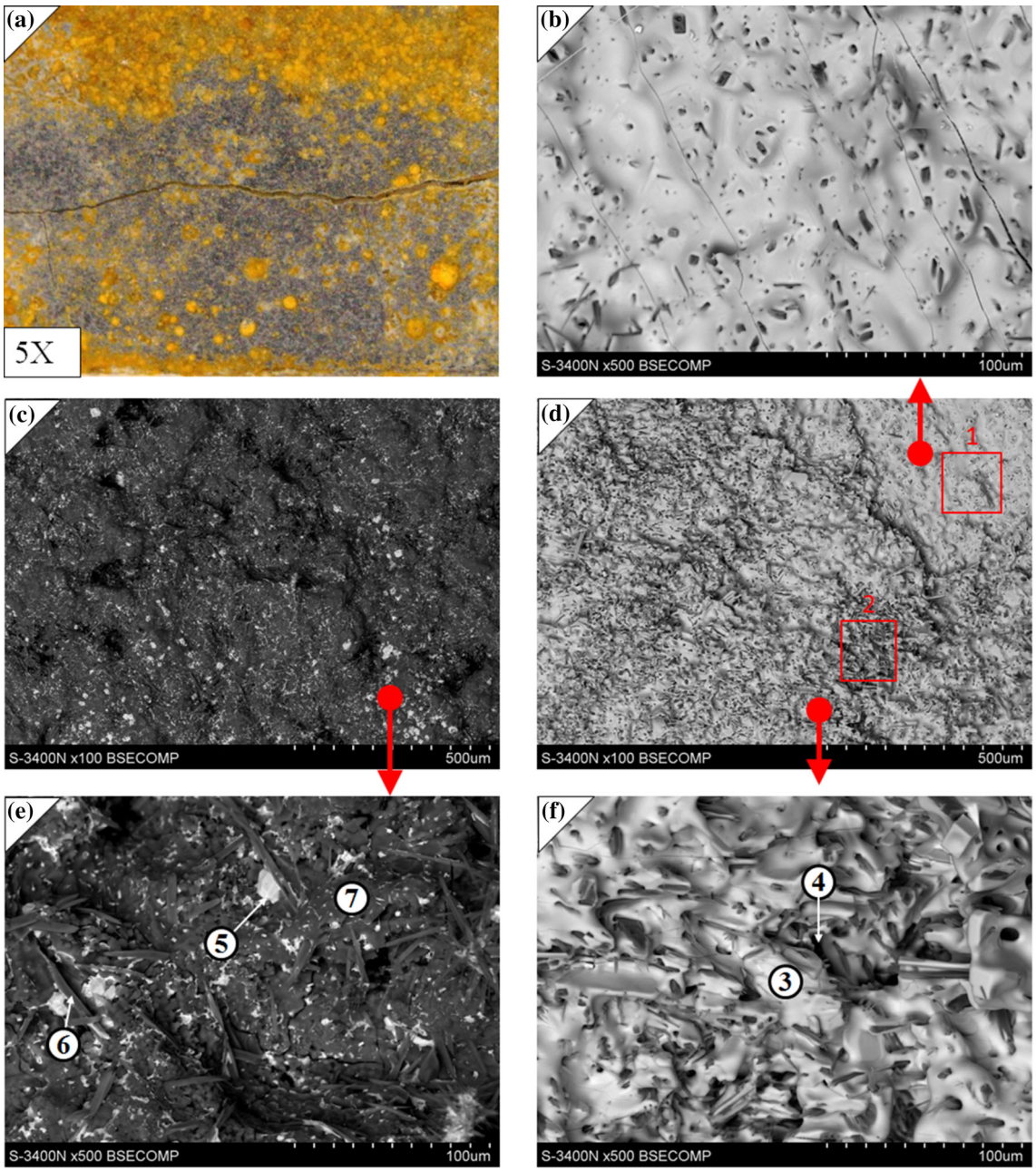

Chemical composition measured in micro areas marked above

Atom %	Mg	Al	Si	Ca	Fe	Zr	Mo	Weight %	Mg	Al	Si	Ca	Fe	Zr	Mo
Area 1	30.3	7.4	2.5	1	0.8	-	58	Area 1	11.1	3	1.1	0.6	0.7	-	83.4
Area 2	24.9	20	6.1	0.8	0.9	-	47.3	Area 2	10.2	9.1	2.9	0.6	0.9	-	76.3
Point 3	4.5	54.8	26.3	-	0.6	-	13.8	Point 3	2.9	40.3	20	-	0.9	-	35.9
Point 4	29.3	11.9	4	-	-	-	54.8	Point 4	11.1	5	1.8	-	-	-	82.3
Point 5	-	2.9	55.4	0.6	-	41.1	-	Point 5	-	1.5	28.7	0.5	-	69.3	-
Point 6	0.3	39.7	57.2	0.5	0.4	-	1.9	Point 6	0.2	36.8	55.3	0.6	0.8	-	6.3
Point 7	1	2.3	90.3	1	-	-	5.4	Point 7	0.7	2	79.9	1.2	-	-	16.2

Fig. 17 SEM/EDS analysis of the surface of siliconized Mo-15Re after oxidation at 1100 °C for 25 h

XRD data and the literature, the mentioned intermediate layer is believed to be Mo_5Si_3 phase.

Because of the phase composition, the siliconized coatings were mainly composed of in situ formed (Mo, Re)Si_2 and $ReSi_{1.75}$ phases. The diffusional character

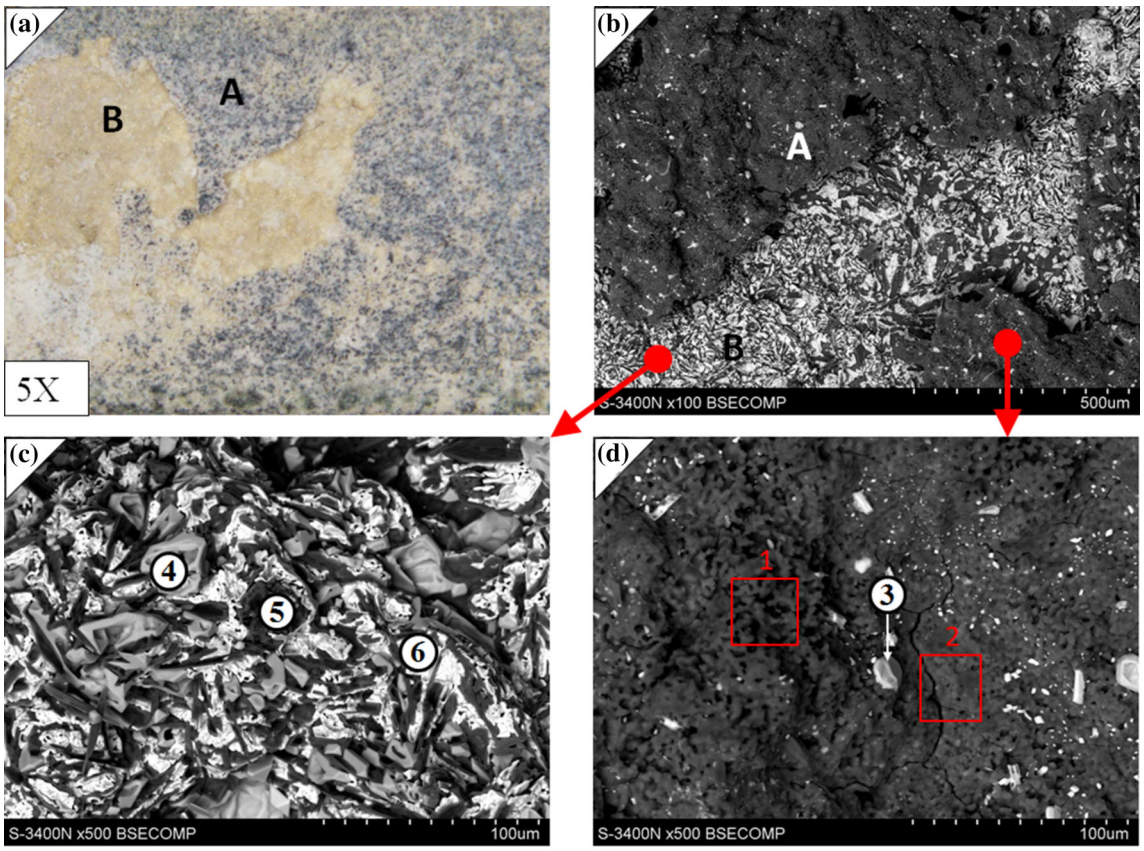

Chemical composition measured in micro areas marked above

Atom %	Al	Si	Fe	Zr	Mo	Weight %	Al	Si	Fe	Zr	Mo
Area 1	1.4	97.4	-	-	1.2	Area 1	1.4	94.6	-	-	4
Area 2	1.5	96.7	-	-	1.8	Area 2	1.3	92.7	-	-	6
Point 3	1	56.3	-	42.7	-	Point 3	0.5	28.7	-	70.8	-
Point 4	11.2	43.2	-	45.6	-	Point 4	5.3	21.4	-	73.3	-
Point 5	54.6	32.4	1.3	11.7	-	Point 5	41.8	25.9	2	30.3	-
Point 6	16.6	13.4	-	70	-	Point 6	6.2	5.2	-	88.6	-

Fig. 18 SEM/EDS analysis of the surface of siliconized Mo-44Re after oxidation at 1100 °C for 25 h

between Mo and Re silicides influenced on a higher concentration of the desired tetragonal $C11_b$ silicide in Mo-Re coatings compared to that of formed on the pure Mo layer. The Mo coating siliconized under the same conditions was characterized by a lower amount of the tetragonal phase at the expense of hexagonal $MoSi_2$. The substitution of Re for Mo in the case of $MoSi_2$ phase is also beneficial taking into account the mechanical properties, especially at high temperatures (Ref 35, 36, 43). Misra et al. reported the enhancement of hardness at room temperature by 30% due to the substitution of 7.5% Re for Mo and up to 100% of increase at 1300 °C (Ref 35). Moreover, the small Re-additions caused the considerable enhancement of the compressive yield strength of the polycrystalline $MoSi_2$ phase up to 1600 °C (Ref 43). The discussed effects connected with rapid solution hardening of $MoSi_2$ by substitutional Re alloying confirm the high potential of (Mo-Re)-$(Mo,Re)Si_2$ gradient coatings because of the high-temperature performance.

The oxidation experiment concerning both siliconized coatings was carried out. Generally, the condition of specimens after 25 h of oxidation at 1000 and 1100 °C was acceptable. The substantial differences in the durability of both coatings under high-temperature oxidation did not occur. The surface condition in all cases was comparable; however, for Mo-15Re (wt.%) coating, some elongated cracks on the surface occurred. Both coatings did not maintain the basic properties during oxidation at 1200 °C, which resulted in a failure of coatings and cracking of the substrate material. It is worth noticing that the decomposition of material occurred upon cooling from high temperature. The coating is therefore exposed to the

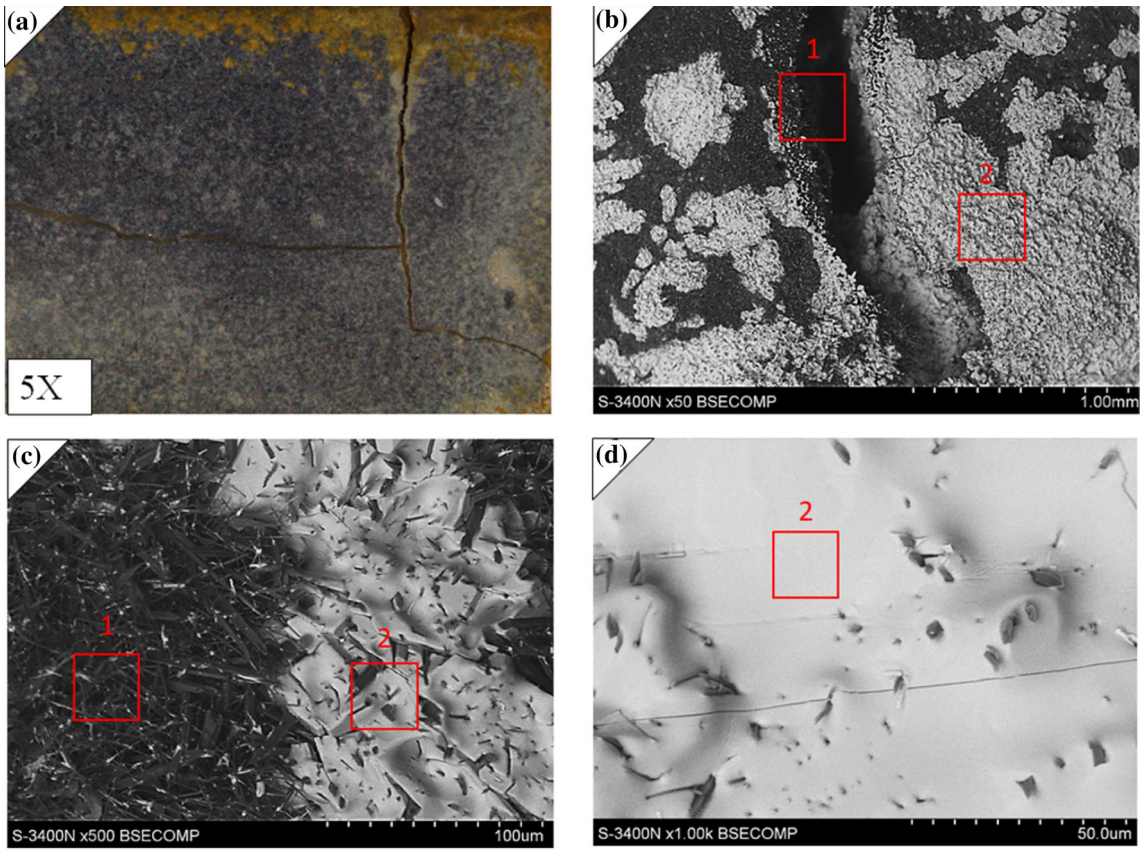

Chemical composition measured in micro areas marked above

Atom %	Mg	Al	Si	Ca	Mo	Weight %	Mg	Al	Si	Ca	Mo
Area 1	1.5	4.3	76.5	1.8	16.3	Area 1	1.5	5.0	86.6	1.4	5.4
Area 2	28.8	13.7	4.7	0.7	52.1	Area 2	11.3	6.0	2.1	0.4	80.2

Fig. 19 SEM/EDS analysis of the surface of siliconized Mo after oxidation at 1100 °C for 25 h

detrimental tensile stresses, whereas in the case of glass processing, the coating is subjected to more beneficial compressive stresses. Moreover, under glass industry conditions, the elements are being replaced after each single production cycle. The character of the scale grown on the siliconized coatings was briefly described. The top oxidized layer was mainly composed of silicon and oxygen that imply the dominance of SiO_2, the typical oxide formed after oxidation of silicide phases.

Because of glass applications, the results of oxidation experiments were satisfactory. The main task of material used under these extremely detrimental conditions is to withstand the life cycle of a single tool, which generally lasts no more than one day. Thus, the investigated gradient coatings may be more beneficial related to currently used solutions. Moreover, this type of surface protection is also favorable taking into account economic aspects and the performance of a coating process. Figure 22 shows potential ways to improve the durability of the elements dedicated to glass melting. The first possibility is based on the deposition of $MoSi_2$ coatings. The disadvantage of such a method is a high price and particularly low availability of commercial $MoSi_2$ powders dedicated for thermal spraying. Moreover, it would be especially difficult to purchase Re-alloyed $MoSi_2$ powders. The second method, according to this paper, is the deposition of Mo-Re (or Mo) coating via plasma spraying and diffusional Si-enrichment to form gradient (Mo, Re)-(Mo, Re)Si_2 or Mo-$MoSi_2$ coatings. Taking into account the industrial conditions, the formation of silicide layers on Mo and Mo-Re coatings could be performed via other methods, including thermal spraying or just a slurry method. The Mo-based coating may be deposited via various commercially available thermal spraying techniques. In the case of glass industry applications, the proposed way of silicon deposition does not require any additional annealing. The elements and tools for glass melting must be slowly heated to temperatures over 1000 °C before contact with the molten glass. Thereby, the diffusional processes between the Mo coating and Si-based slurry may occur during heating, resulting in

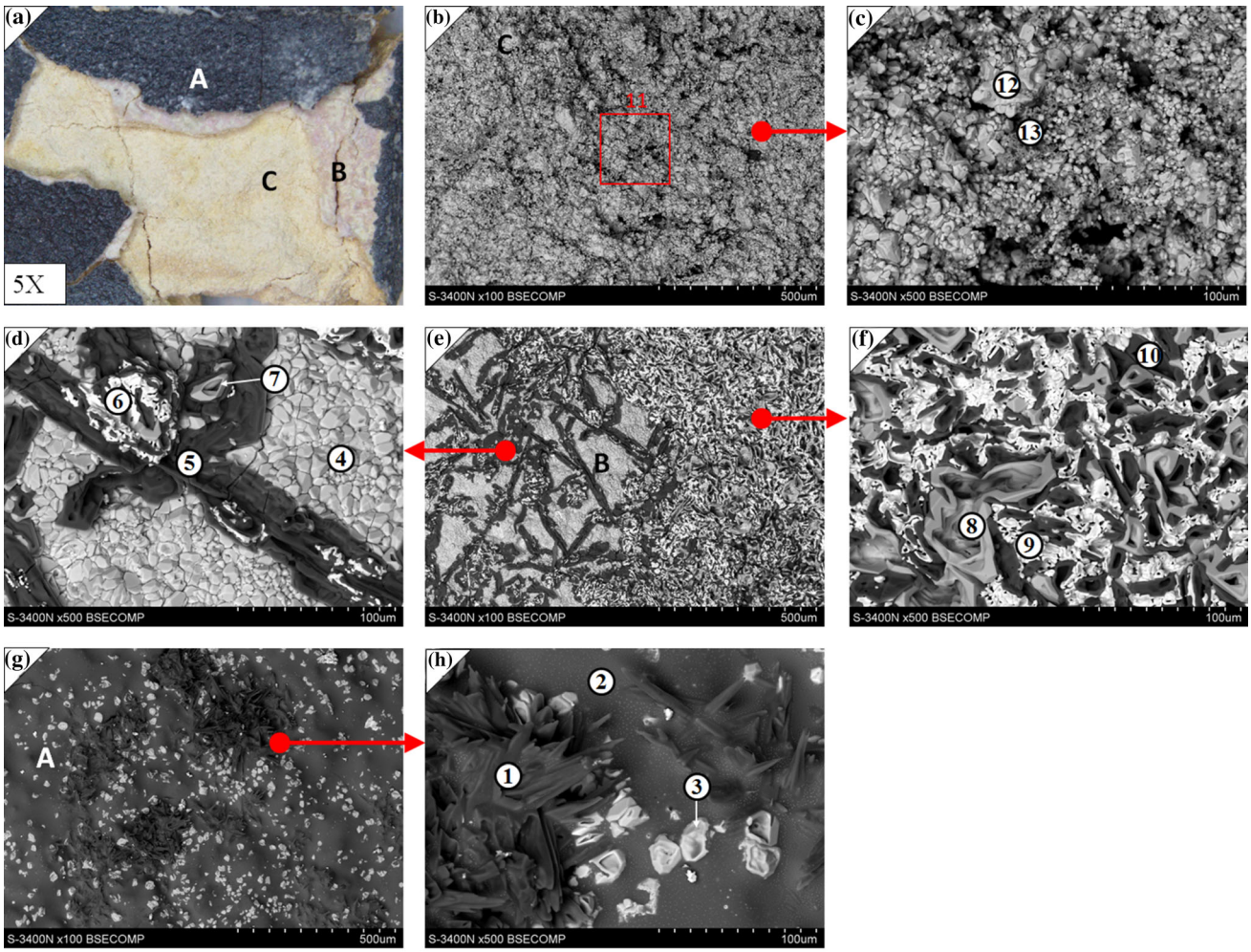

Chemical composition measured in micro areas marked above

Atom %	Na	Al	Si	K	Ca	Ti	Fe	Zr	Mo	Weight %	Na	Al	Si	K	Ca	Ti	Fe	Zr	Mo
Point 1	0.9	46.7	44.6	1.1	1.1		2	2.2	1.4	Point 1	0.7	41.1	40.8	1.4	1.4		3.6	6.5	4.5
Point 2	2.6	13.8	70.1	4.1	1.7	0.4	1.3	2.4	3.6	Point 2	1.8	11.4	59.9	4.9	2	0.5	2.2	6.8	10.5
Point 3	1.3	6.8	47.5	0.7			-	43.7	-	Point 3	0.5	3.3	24	0.5			-	71.7	-
Point 4	-	10	38.6	-	-	-	-	51.4	-	Point 4	-	4.5	17.9	-	-	-	-	77.6	-
Point 5	-	84.5	3.9	-	-	-	0.8	10.8	-	Point 5	-	66.8	3.2	-	-	-	1.3	28.7	-
Point 6	-	21.1	2.6	-	-	-	-	76.3	-	Point 6	-	7.5	1	-	-	-	-	91.5	-
Point 7	-	15.1	36.7	-	-	-	-	48.2	-	Point 7	-	7	17.7	-	-	-	-	75.3	-
Point 8	-	10.3	38.3	-	-	-	-	51.4	-	Point 8	-	4.6	17.8	-	-	-	-	77.6	-
Point 9	-	49	4.8	-	-	-	-	46.2	-	Point 9	-	23.3	2.4	-	-	-	-	74.3	-
Point 10	-	49.7	10.9	-	-	-	1.7	37.7	-	Point 10	-	25.9	5.9	-	-	-	1.8	66.4	-
Area 11	-	-	15.1	-	-	-	-	84.9	-	Area 11	-	-	5.2	-	-	-	-	94.8	-
Point 12	-	-	5.7	-	-	-	-	94.3	-	Point 12	-	-	1.8	-	-	-	-	98.2	-
Point 13	-	-	32.8	-	-	-	-	67.2	-	Point 13	-	-	13.1	-	-	-	-	86.9	-

Fig. 20 SEM/EDS analysis of the surface of siliconized Mo-15Re after oxidation at 1200 °C for 25 h

the formation of the silicide layer on the material sooner the glass is contacting the tool. This solution allows forming the protective layers on a wide variety of the industrial glass melting tools in an efficient way, because even elements with large dimensions may be coated by a combination of thermal spraying and slurry methods. The

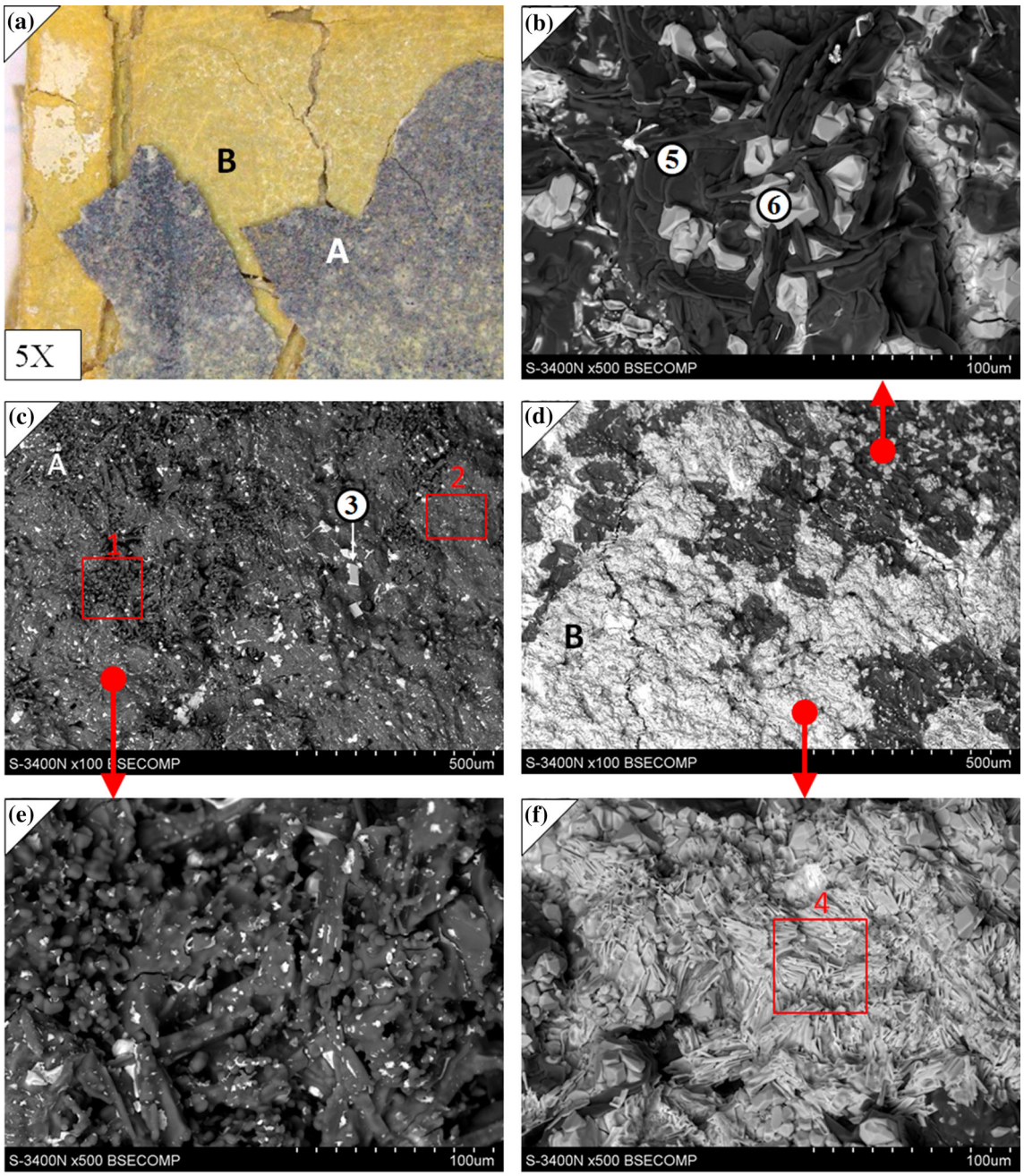

Chemical composition measured in micro areas marked above

Atom %	Mg	Al	Si	Zr	Mo	Weight %	Mg	Al	Si	Zr	Mo
Area 1	1.7	2.5	90.9	-	4.9	Area 1	1.3	2.2	81.4		15.1
Area 2	10.5	25.1	58.5	-	5.9	Area 2	8.1	21.5	52.4		18
Point 3	34.1	5.5	12.4	-	48	Point 3	14	2.5	5.9	0	77.6
Area 4	24.5	13.6	3.1	3.5	55.3	Area 4	8.9	5.5	1.3	4.8	79.5
Point 5	-	91.3	4	4.7	-	Point 5	-	81.9	3.8	14.3	-
Point 6	-	15.9	38.2	45.9	-	Point 6	-	7.6	18.8	73.6	-

Fig. 21 SEM/EDS analysis of the surface of siliconized Mo-44Re after oxidation at 1200 °C for 25 h

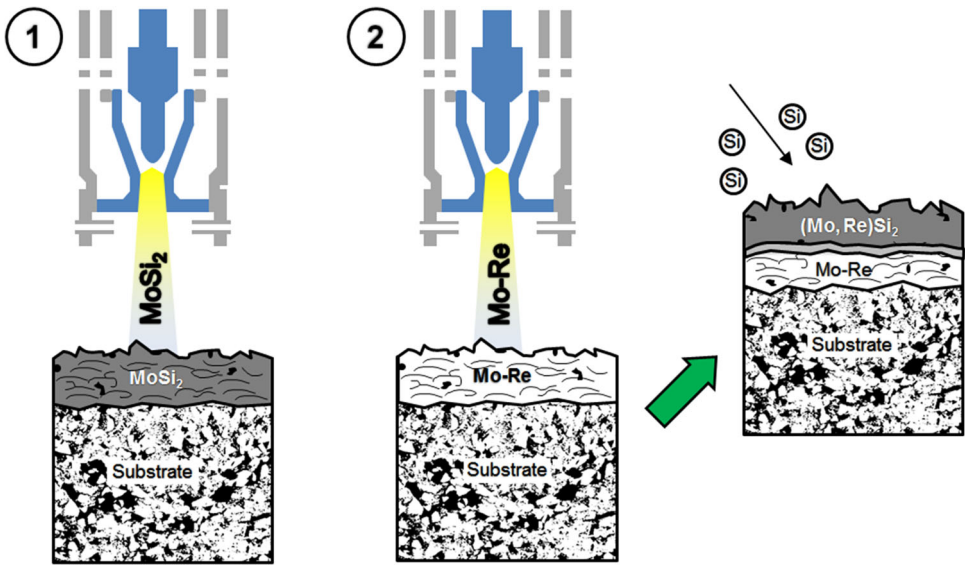

Fig. 22 Potential ways of deposition of molybdenum silicide coatings

discussed techniques are commercially available, whereas the siliconizing process takes place simultaneously during the heating of the tools.

Conclusions

The pack siliconizing was performed to improve the oxidation resistance of the new plasma-sprayed Mo-Re coatings dedicated for application in the glass industry. The presence of two characteristic layers characterized both Mo-15Re and Mo-44Re (wt.%) coatings after the siliconizing process. The outer one was (Mo, Re)Si_2-$ReSi_{1.75}$ zone, whereas underneath, the Mo-Re layer was present. Both gradient coatings were deposited on ZrO_2-Mo composite.

Novel (Mo-Re)-(Mo, Re)Si_2 gradient coatings may be more beneficial because of the glass melting application compared to those of $MoSi_2$. Because of the silicide coatings, during the siliconizing process, the desired tetragonal silicide phase may be formed easier in the case of Re-added Mo coating compared to that of pure Mo substrate. Except for the stabilization of the tetragonal $C11_b$ structure, rhenium may improve the high-temperature strength via solution hardening of $MoSi_2$ by substitutional Re alloying (Ref 41). These effects contribute to the high potential of the investigated gradient coatings because of the glass melting applications. The oxidation experiments showed that discussed protective coatings withstand high-temperature oxidation during the time adequate to tools' life cycle.

Furthermore, except for the coatings' characterization, the potentially efficient ways of their deposition in terms of industrial conditions were proposed.

Acknowledgments Publication supported by the Rector's Grant in the field of research and development. Silesian University of Technology, grant number 11/030/RGJ19/0233.

References

1. V.L. Burdick, The Corrosive Nature of Molten Glass, *Introduction to Glass Science*, L.D. Pye, H.J. Stevens, and W.C. LaCourse, Ed., Plenum Press, New York, 1972, p 545-561
2. I. Vanmoortel, J. De Strycker, E. Temmerman, and A. Adriaens, Insights into the Oxidation Mechanism of Molybdenum in Molten Glass, *Ceram.-Silikáty*, 2018, **52**, p 1-7
3. M. Dunk, A. Fantinel, G. Dinelli, and R. Tongon, Molybdenum/Fused Cast AZS Material for Critical Areas in Glass Melting Tanks, *Ceram. Eng. Sci. Proc.*, 1996, **18**, p 216-217
4. R. Duncan, R. Coupland, and P. Williams, New Stirrer Technology for the Glass Industry, *Platin. Met. Rev.*, 2005, **49**, p 62
5. N.I. Min'ko, N.F. Zhernovaya, O.I. Tkachenko, VYu Krasavin, and Z.P. Baskova, The Effect of Process Parameters on the Stability of Molybdenum Electrodes in Glass-Melting Furnace, *Glass Ceram.*, 2000, **57**, p 333-334
6. M. Yamamoto, K. Sakai, R. Akagi, M. Sakai, H. Yamashita, and T. Maekawa, Electrochemical Corrosion of Molybdenum Electrodes in an Aluminosilicate Glass Melt Containing Antimony, *J. Ceram. Soc. Jpn.*, 2004, **112**, p 179-183
7. M. Laribi, A.B. Vannes, and D. Treheux, Study of Mechanical Behavior of Molybdenum Coating Using Sliding Wear and Impact Tests, *Wear*, 2007, **262**, p 1330-1336
8. T.A. Stolarski and S. Tobe, The Effect of Spraying Distance on Wear Resistance of Molybdenum Coatings, *Wear*, 2001, **249**, p 1096-1102
9. H. Byoungchul, L. Sunghak, and A. Jeehoon, Correlation of Microstructure and Wear Resistance of Molybdenum Blend

Coatings Fabricated by Atmospheric Plasma Spraying, *Mater. Sci. Eng., A*, 2004, **366**, p 152-163
10. A.P. Tomiisa, E. Saiz, S. Lopez-Esteban, M. Benhassine, J. de Coninck, N. Rauch, and M. Ruhle, Wetting of Metals and Glasses on Mo, *Int. J. Mater. Res.*, 2007, **98**, p 1238-1243
11. E.R. Braithwaite and J. Haber, *Molybdenum: An Outline of its Chemistry and Uses*, Elsevier, Amsterdam, 1994
12. S.A. Fabritsiev, V.A. Gosudarenkov, V.A. Potapova, V.V. Rybin, L.S. Kosachev, V.P. Chakin, A.S. Pokrovsky, and V.R. Barabash, Effects of Neutron Irradiation on Physical and Mechanical Properties of Mo-Re Alloys, *J. Nucl. Mater.*, 1992, **191–194**, p 426-429
13. J.A. Shields, Jr., *Application of Molybdenum Metal and Its Alloys*, International Molybdenum Association, London, 2013
14. M. Osadnik, A. Wrona, M. Lis, M. Kamińska, K. Bilewska, M. Czepelak, K. Czechowska, G. Moskal, and G. Więcław, Plasma-Sprayed Mo-Re Coatings for Glass Industry Applications, *Surf. Coat. Technol.*, 2017, **318**, p 349-354
15. A.V. Krajnikov, A.S. Drachinskiy, V.N. Slyunyayev, and V.N. Slyunyayev, Grain Boundary Segregation in Recrystallized Molybdenum Alloys and Its Effect on Brittle Intergranular Fracture, *Int. J. Refract Metal Hard Mater.*, 1992, **11**, p 175-180
16. H. Kurishita, Y. Kitsunai, T. Shibayama, H. Kayano, and Y. Hiraoka, Mo Alloys with Improved Resistance to Embrittlement by Recrystallization and Irradiation, *J. Nucl. Mater.*, 1996, **233–237**, p 557-564
17. Y. Hiraoka, M. Okada, and H. Irie, Alloying to Improve the Properties of Welded Molybdenum, *J. Nucl. Mater.*, 1988, **155–157**, p 381-385
18. P. Falbriard, P. Rochette, and G. Nicolas, Refractory Materials Likely to be Used in the NET Divertor Armour, *Int. J. Refract Metal Hard Mater.*, 1991, **10**, p 37-43
19. K.J. Leonard, J.T. Busby, and S.J. Zinkle, Microstructural and Mechanical Property Changes with Aging of Mo–41 Re and Mo–47.5 Re Alloys, *J. Nucl. Mater.*, 2007, **366**, p 369-387
20. N.N. Morgunova, A.V. Abramyan, and N.I. Kazakova, Effect of Rhenium on the Brittle Fracture Threshold of Molybdenum, *Met. Sci. Heat Treat.*, 1987, **29**, p 441-447
21. A. Krajnikov, F. Morito, and M. Danylenko, Rhenium Effect in Irradiated Mo-Re Alloys and Welds, *Univ. J. Mater. Sci.*, 2014, **2**, p 19-26
22. S.A. Fabritsiev and A.S. Pokrovsky, The Effect of Rhenium on the Radiation Damage Resistivity of Mo–Re Alloys, *J. Nucl. Mater.*, 1998, **252**, p 216-227
23. A. Wrona, M. Lis, M. Osadnik, M. Kamińska, K. Bilewska, K. Czechowska, G. Więcław, and G. Moskal, Warstwy ochronne na bazie metali wysokotopliwych wytwarzane techniką natryskiwania cieplnego, *Obróbka Plastyczna Metali*, 2015, **2**, p 177-190
24. R.W. Bartlett, Molybdenum Oxidation Kinetics at High Temperatures, *J. Electrochem. Soc.*, 1965, **112**, p 744-746
25. E.A. Gulbransen, K.F. Andrew, and F.A. Brasset, Oxidation of Molybdenum 550° to 1700 °C, *J. Electrochem. Soc.*, 1963, **110**, p 952-959
26. T. Karahana, G. Ouyang, P.K. Ray, M.J. Kramer, and M. Akinc, Oxidation Mechanism of W Substituted Mo-Si-B Alloys, *Intermetallics*, 2017, **87**, p 38-44
27. Y.Y. Zhang, W.J. Ni, and Y.G. Li, Effect of Siliconizing Temperature on Microstructure and Phase Constitution of Mo–$MoSi_2$ Functionally Graded Materials, *Ceram. Int.*, 2018, **44**, p 11166-11171
28. Y.Y. Zhang, J. Zhao, J.H. Li, J. Lei, and X.K. Cheng, Effect of Hot-Dip Siliconizing Time on Phase Composition and Microstructure of Mo–$MoSi_2$ High Temperature Structural Materials, *Ceram. Int.*, 2019, **45**, p 5588-5593
29. J.A. Hawk and D.E. Alman, A Comparative Study of the Abrasive Wear Behavior of $MoSi_2$, *Scr. Metall. Mater.*, 1995, **32**, p 725-730
30. J. Yan, Z. He, Y. Wang, J. Qiu, and Y. Wang, Microstructure and Wear Resistance of Plasma-Sprayed Molybdenum Coating Reinforced by $MoSi_2$ Particles, *J. Therm. Spray Technol.*, 2016, **25**, p 1322-1329
31. Y.Y. Zhang, Y.G. Li, and C.G. Bai, Microstructure and Oxidation Behavior of Si–MoSi2 Functionally Graded Coating on Mo Substrate, *Ceram. Int.*, 2017, **43**, p 6250-6256
32. P. Mao, H. Kan, and Y. Xin, Thermodynamic Assessment of the Mo–Re Binary System, *J. Alloy. Compd.*, 2008, **464**, p 190-196
33. J.K. Yoon, J.K. Lee, K.H. Lee, J.Y. Byun, G.H. Kim, and K.T. Hong, Microstructure and Growth Kinetics of the Mo_5Si_3 and Mo_3Si Layers in $MoSi_2$/Mo Diffusion Couple, *Intermetallics*, 2003, **11**, p 687-696
34. T. Siegrist, F. Hulliger, and G. Travaglini, The Crystal Structure and Some Properties of ReSi2, *J. Less Common Met.*, 1983, **92**, p 119-129
35. T.E. Mitchell and A. Misra, Structure and Mechanical Properties of (Mo, Re)Si_2 Alloys, *Mater. Sci. Eng., A*, 1999, **261**, p 106-112
36. Y. Harada, Y. Murata, and M. Morinaga, Solid solution Softening and Hardening in Alloyed $MoSi_2$, *Intermetallics*, 1998, **6**, p 529-535
37. F.M. d'Heurle, C.S. Petersson, and M.Y. Tsai, Observations on the Hexagonal Form of $MoSi_2$ and WSi_2 Films Produced by ion Implantation and on Related Snowplow Effects, *J. Appl. Phys.*, 1980, **51**, p 5976-5980
38. U. Gottlieb, B. Lambert-Andron, F. Nava, M. Affronte, O. Laborde, A. Rouault, and R. Madar, Structural and Electronic Transport Properties of $ReSi_2 - \delta$ Single Crystals, *J. Appl. Phys.*, 1995, **78**, p 3902-3907
39. A.N. Qiu, L. Zhang, and J. Wu, Structure Stability and Electronic Structure of Semiconducting Rhenium Silicide with Doping, *Adv. Mater. Res.*, 2007, **26–28**, p 1029-1032
40. L. Pawlowski, *The Science and Engineering of Thermal Spray Coatings*, Wiley, New York, 1995
41. M.Z. Mehrizi, M. Shamanian, A. Saidi, R.S. Razazvi, and R. Beigi, Evaluation of Oxidation Behavior of Laser Clad CoWSi-WSi_2 Coating on Pure Ni Substrate at Different Temperatures, *Ceram. Int.*, 2015, **41**, p 9715-9721
42. P. Zhang and X. Guo, Improvement in Oxidation Resistance of Silicide Coating on an Nb-Ti-Si Based Ultrahigh Temperature Alloy by Second Aluminizing Treatment, *Corros. Sci.*, 2015, **91**, p 101-107
43. A. Misra, A.A. Sharif, J.J. Petrovic, and T.E. Mitchell, Rapid Solution Hardening at Elevated Temperatures by Substitutional Re Alloying in $MoSi_2$, *Acta Mater.*, 2000, **48**, p 925-932